

ARMY RESEARCH LABORATORY



Modeling Threshold Velocity of Hemispherical and Ogival-Nose Tungsten-Alloy Penetrators Perforating Finite Aluminum Targets

by Daniel R. Scheffler

ARL-TR-1583

January 1998

DTIC QUALITY INSPECTED 2

19980129 017

Approved for public release; distribution is unlimited.

The findings in this report are not to be construed as an official Department of the Army position unless so designated by other authorized documents.

Citation of manufacturer's or trade names does not constitute an official endorsement or approval of the use thereof.

Destroy this report when it is no longer needed. Do not return it to the originator.

Army Research Laboratory

Aberdeen Proving Ground, MD 21005-5066

ARL-TR-1583

January 1998

Modeling Threshold Velocity of Hemispherical and Ogival-Nose Tungsten-Alloy Penetrators Perforating Finite Aluminum Targets

Daniel R. Scheffler

Weapons and Materials Research Directorate, ARL

Abstract

This study examines the ability of the CTH hydrocode to predict the effect of rod nose-shape on the transition from rigid body to eroding rod penetration for tungsten alloy long-rod penetrators perforating finite aluminum targets. Two rod nose-shapes and two target alloys were considered. The rod nose-shapes were hemispherical and ogival, and the target alloys were 7.62-cm-thick 5083 and 7039 aluminum. Results are compared to an experimental study that delineated the effect of nose-shape on the threshold velocity at which tungsten alloy penetrators transition from rigid body to eroding rod when perforating finite aluminum targets.

Acknowledgments

The author would like to thank Dr. Steven B. Segletes and Mr. Kent D. Kimsey for their helpful comments and suggestions regarding this paper. The author would especially like to thank Dr. Lee S. Magness, Jr. for discussions regarding his experiments and assuring the accuracy of the discussions of them. Additional thanks go to Dr. Stewart A. Silling of Sandia National Laboratories for discussions regarding his boundary layer interface algorithm and for providing an advanced copy of parts of his user manual.

INTENTIONALLY LEFT BLANK.

Table of Contents

	<u>Page</u>
Acknowledgments	iii
List of Figures	vii
List of Tables	ix
1. Introduction	1
2. Problem Setup	3
3. Results and Discussion	6
3.1 Residual Shapes for Baseline Simulations	8
3.2 Residual Velocity for Baseline Simulations	14
3.3 BLINT Model Parameters	17
3.4 Failure Model Effects	20
4. Conclusions	22
5. References	29
Appendix A: Input for Hemi-Nose KE-BL-CO-P Sims vs. 5083 Aluminum Targets - Changes for MV, NB, and NC Sims Given in Notes ..	33
Appendix B: Input for Ogival-Nose KE-BL-CO-P Sims vs. 5083 Aluminum Targets - Changes for MV, NB, and NC Sims Given in Notes ..	41
Appendix C: Input for Hemi-Nose KE-BL-CO-P Sims vs. 7039 Aluminum Targets - Changes for MV, NB, and NC Sims Given in Notes ..	49
Appendix D: Input for Ogival-Nose KE-BL-CO-P Sims vs. 7039 Aluminum Targets - Changes for MV, NB, and NC Sims Given in Notes ..	57
Appendix E: Input for Hemi-Nose KE-BL-CO-S Sims vs. 5083 Aluminum Targets	65
Appendix F: Input for Ogival-Nose KE-BL-CO-S Sims vs. 5083 Aluminum Targets	73

	<u>Page</u>
Appendix G: Table of Simulation Results	81
Distribution List	85
Report Documentation Page	91

List of Figures

<u>Figure</u>	<u>Page</u>
1. Penetrator Geometries	3
2. Comparison of Hemi-Nose Penetrator KE and MV Sims Residual Shapes With Experiment After Perforating 5083 Aluminum Targets	9
3. Comparison of Hemi-Nose Penetrator KE and MV Sims Residual Shapes With Experiment After Perforating 7039 Aluminum Targets	10
4. Residual Shapes of the Ogival-Nose Penetrator KE Sims After Perforating 5083 Aluminum Targets	12
5. Residual Shapes of the Ogival-Nose Penetrator MV Sims After Perforating 5083 Aluminum Targets	13
6. Experimentally Determined Residual Shapes of the Ogival-Nose Penetrator After Perforating 7039 Aluminum Targets	14
7. Residual Shapes of the Ogival-Nose Penetrator KE Sims After Perforating 7039 Aluminum Targets	15
8. Residual Shapes of the Ogival-Nose Penetrator MV Sims After Perforating 7039 Aluminum Targets	16
9. Residual Velocity Comparison Between Experiment, KE, and MV Sims After Perforating 5083 Aluminum Targets	17
10. Residual Velocity Comparison Between Experiment, KE, and MV Sims After Perforating 7039 Aluminum Targets	18
11. Residual Shapes of KE-NB-NC-P Sims After Perforating 5083 Aluminum Targets	19
12. Comparison of Residual Velocity for KE-NB-NC-P Sims With Experiment and Baseline KE Sims After Perforating 5083 Aluminum Targets	20
13. Residual Shapes for Hemi-Nose Penetrator KE-BL-NC-P Sims After Perforating 5083 Aluminum Targets	21

<u>Figure</u>		<u>Page</u>
14.	Residual Shapes for Ogival-Nose Penetrator KE-BL-NC-P Sims After Perforating 5083 Aluminum Targets	22
15.	Comparison of Residual Velocity for KE-BL-NC-P Sims With Experiment and Baseline KE Sims After Perforating 5083 Aluminum Targets	23
16.	Residual Shapes for Hemi-Nose Penetrator KE-BL-CO-S Sims After Perforating 5083 Aluminum Targets	24
17.	Residual Shapes for Ogival-Nose Penetrator KE-BL-CO-S Sims After Perforating 5083 Aluminum Targets	25
18.	Comparison of Residual Velocity for KE-BL-CO-S Sims With Experiment and Baseline KE Sims After Perforating 5083 Aluminum Targets	26

List of Tables

<u>Table</u>	<u>Page</u>
1. Equation-of-State Parameters	4
2. Initial Impact Conditions and Ballistic Test Results	7

INTENTIONALLY LEFT BLANK.

1. Introduction

In examining the convergence characteristics of the Eulerian CTH hydrocode [1] as a function of spatial resolution, Zukas [2] found that the code could not accurately predict perforation of armor plate by a hard projectile at low velocities (less than 1.5 km/s). A penetrator, which, in experiments, perforated a finite steel target with significant residual length and velocity, was predicted to be unable to perforate the target. Previously, this problem had been modeled successfully using an in-house version of the EPIC Lagrangian hydrocode. Zukas observed that, regardless of the mixed cell strength formulation used (several are available in the CTH hydrocode), high-strength penetrator material included in a mixed cell was modeled as being significantly softer—an unrealistic treatment that caused excessive deformation in the penetrator. The net effect was that the CTH hydrocode could not accurately model the rigid-body penetration of a soft target, an eroding projectile penetrating harder targets at low velocities or the sliding between two material interfaces.

A new boundary layer algorithm for sliding interfaces (BLINT) was recently incorporated into the CTH hydrocode for two-dimensional problems only [3]. The algorithm relocates the slip layer outside of mixed cells into the softer material, thus allowing hard materials to penetrate as rigid bodies. Good correlation with experiments has been obtained using the BLINT algorithm by Silling [4] and Kmetyk and Yarrington [5]. Both modeled hard penetrators impacting soft targets knowing, a priori, that the penetrators would remain rigid.

This study examined the ability of the CTH hydrocode (August 1993 release) to predict the impact velocity at which a penetrator would transition from rigid-body to eroding-rod, the effect of the rod's nose shape on this transition velocity and its residual velocity and shape while perforating finite aluminum targets. The perforation of soft aluminum targets by tungsten alloy (95W-2.5Ni-1.0Fe-1.5Co, cold worked by swaging to a 21% reduction in area) long rods was modeled. To gauge the accuracy of the CTH hydrocode with the BLINT algorithm, the simulation results were compared to the experimentally determined residual penetrator velocity and shape [6].

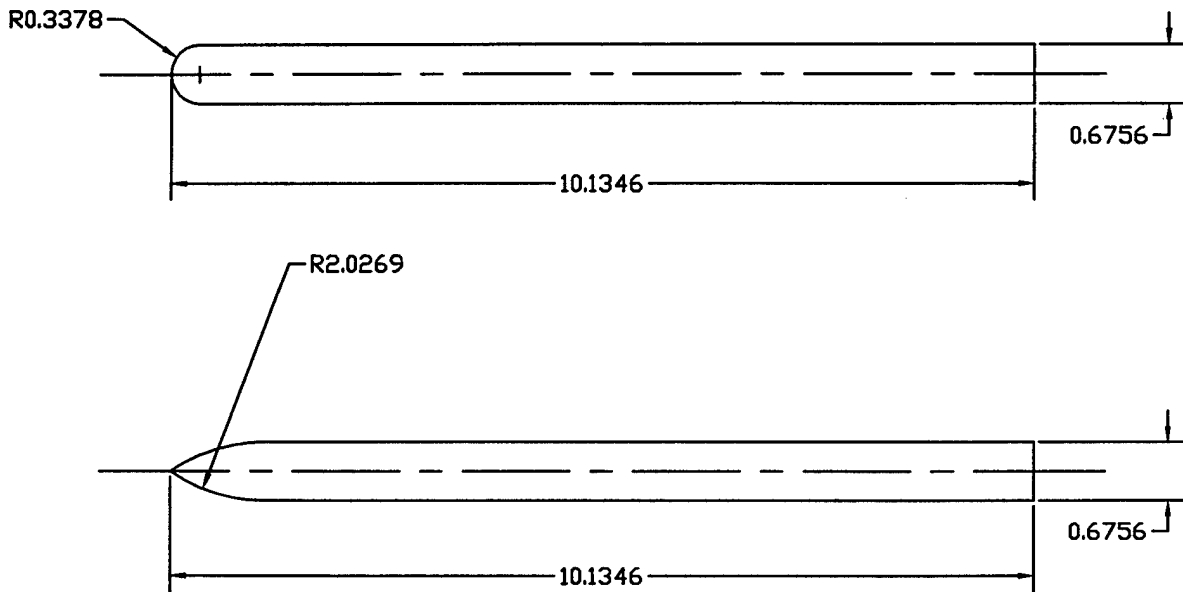
Two rod nose-shapes and two target alloys were considered. The rod nose-shapes were hemispherical and ogival, and the target alloys were 7.62-cm (3 in)- thick 5083 and 7039 aluminum.

A subset of the results of this study first appeared at the Symposium on Structures Under Extreme Loading Conditions as part of the 1996 ASME Pressure Vessel and Piping Conference that took place in Montreal, Canada from 21–26 July 1996 [7]. A companion paper [8] and report [9] also exist, which provide the simulation results for impacts with 53.34-cm-thick aluminum targets where results are compared with experimental depth-of-penetration (DOP) tests. The companion report provides more detail than the companion paper. This report differs from the original paper by including additional simulations and experiments, a more detailed discussion of the BLINT model, the examination of effective plastic strains, as well as the input decks used for the simulations.

The CTH hydrocode is a state-of-the-art, second-order accurate, Eulerian hydrocode developed by Sandia National Laboratories which is capable of solving complex problems in shock physics in one, two, or three dimensions. The code provides several constitutive models, including an elastic-perfectly plastic model with provisions for work hardening and thermal softening, the Johnson-Cook model [10], the Zerrilli-Armstrong model [11], the Steinberg-Guinan-Lund model [12, 13], and an undocumented power-law model. High-explosive detonation can be modeled using the programmed burn model, the Chapman-Jouguet volume burn models, or the history variable reactive burn model [14]. Several equation-of-state (EOS) options are available, including tabular (i.e., SESAME), analytical (ANEOS), Mie-Grüneisen, and Jones-Wilkins-Lee (JWL) [15]. Material failure occurs when a threshold value of tensile stress or hydrostatic pressure is exceeded. In addition, the Johnson-Cook failure model [16] is also available. When failure occurs in a cell, void is introduced until the stress state of the cell is reduced to zero. Recompression is permitted. To reduce the diffusion typically encountered in Eulerian simulations, several advanced material interface tracking algorithms are provided, including the high-resolution interface tracking (HRIT) algorithm (available for two-dimensional simulations only), the simple line interface calculation (SLIC) algorithm [17], and the Sandia-modified Young's reconstruction algorithm (SMYRA) [18].

2. Problem Setup

The two geometries for the tungsten alloy penetrators are shown in Figure 1. Both of the penetrators have a length of 10.1346 cm (3.99 in) and a diameter of 0.6756 cm (0.266 in). Due to their different nose shapes, the masses of the penetrators differ slightly. The mass of the hemi-nose penetrator is approximately 65 g, and that of the ogival-nose penetrator is approximately 63 g.



All Dimensions Are In Centimeters

Figure 1. Penetrator Geometries.

Three different constitutive models were used in the simulations to model the deviatoric response of the materials. The choice of the constitutive model used for a material was governed by the availability of material data. Material data were not available for the 95W-2.5Ni-1.0Fe-1.5Co, 21% swaged tungsten alloy penetrators used in the experiments. Therefore, the alloy was approximated using 95W-3.5Ni-1.5Fe tungsten alloy data for the Steinberg-Guinan-Lund strain-rate-independent model reported in Steinberg [19]. This tungsten alloy has the same percentage of tungsten and same approximate density as the 95W-2.5Ni-1.0Fe-1.5Co, 21% swaged alloy. For the 7039 aluminum

target, the Johnson-Cook constitutive model was used with the parameters reported in Johnson and Cook [10]. For the 5083 aluminum target, a power-law constitutive model was used with the parameters reported in Silling [3] and originally reported in Forrestal et al. [20].

The Mie-Grüneisen EOS was used for all materials. EOS data were obtained from a data file provided with the CTH hydrocode. The EOS parameters for 5083 aluminum, 7039 aluminum, and 95% tungsten content tungsten alloy were not available. Therefore, they were approximated using parameters for 6061 aluminum, 7075 aluminum, and 90W-7Ni-3Fe tungsten alloy, respectively. The initial densities of the 6061 and the 7075 aluminum alloys were changed to reflect those for 5083 and 7039 aluminum, as reported in the Metals Handbook Desk Edition [21]. The initial density of the 90W-7Ni-3Fe alloy was changed to reflect the initial density of the 95W-3.5Ni-1.5Fe alloy reported in Steinberg [19]. The EOS parameters used for the materials are listed in Table 1.

Table 1. Equation-of-State Parameters

Material	Density ρ_0 (g/cm ³)	Sound Speed c_0 (km/s)	Slope Us-Up (s)	Grüneisen Parameter (Γ_0)	Specific Heat c_v (erg/g/eV)
W Alloy	18.16	4.03	1.237	1.67	1.66e10
5083 Al	2.66	5.34	1.40	1.97	1.07e11
7039 Al	2.77	5.20	1.36	2.20	1.07e11

Failure in most of the simulations was modeled using a threshold-pressure criterion. The tensile pressure at which the tungsten alloy, the 5083 aluminum, and the 7039 aluminum were assumed to fail was 3.5, 0.45, and 0.50 GPa, respectively. Additional simulations used a strain-based failure criterion that is described later in this report.

All simulations used a two-dimensional cylindrical coordinate mesh consisting of 85×832 cells. The mesh in the radial direction starts at the axis of symmetry with a constant cell size of 0.0422275 cm out to a radius of 1.6891 cm. Thereafter, cell dimensions expand by 5% increments

out to the outer radius of the target. This mesh provides eight cells across the radius of the penetrator. The mesh in the axial direction mesh has a constant cell size of 0.0422275 cm. Thus, cells in the penetrator-target interaction region have a one-to-one aspect ratio.

Parameters for the BLINT model were chosen to be similar to those reported in Kmetyk and Yarrington [5]. Thus, the boundary-layer distance (w_{bl}) and the slip-layer distance (w_{sl}) were chosen to be twice the zone size of cells in the penetrator-target interaction region. The boundary-layer distance defines which cells will be included in the boundary layer. If the cell center of a cell is located w_{bl} away from a cell whose center is included in the interface layer, it is considered to be part of the boundary layer. Materials defined as "hard" make up the hard boundary layer and materials defined as "soft" make up the soft boundary layer. The interface layer, which is about two cell widths thick, contains all cells whose hard and soft material volume vector gradient magnitudes are both greater than or equal to 0.1. The slip-layer distance defines which cells will be included in the slip layer. If the cell center of a cell located in the soft boundary layer is w_{sl} from a cell whose center is included in the interface layer, it is considered part of the slip layer. Cells located in the slip layer have their flow stresses set to zero, allowing sliding to occur in these cells. An option to automatically increase the yield strength of the penetrator material by a factor equal to

$$\left(\frac{r_o + w_{bl}}{r_o} \right)^2$$

(where r_o is the outer radius of the penetrator) was used. This ratio represents the cross-sectional area of the penetrator plus the boundary-layer distance over the original penetrator cross-sectional area. The option was used because numerical noise can cause shear stresses close to the yield stress to exceed the yield stress, causing premature irreversible deformation of the penetrator. An additional option allows for the inclusion of friction; however, friction between the target and penetrator was not accounted for in this study. Kmetyk and Yarrington [5] showed that the BLINT model tended to overpredict penetration in deep penetration problems unless friction was included.

The CTH hydrocode (August 1993 version) cannot convect velocity in a manner such that both momentum (MV) and kinetic energy (KE) are both conserved exactly. The default option allows

conservation of KE such that total energy is conserved during the convection phase of a computational cycle; however, MV is not conserved. A second option convects velocity such that MV is conserved during the convection phase of a computational cycle and any KE discrepancies are discarded. Simulations were run for both of these convection options. A final option conserves both MV and total energy during the convection phase of a computational cycle by depositing the KE discrepancy into internal energy. This can have the effect of artificially heating a material [22], and therefore, this option was not used. (Note: With the March 1995 release of the code, a half index shifted momentum scheme was introduced as the only convection option, thus the choice of convection options discussed previously are no longer available in code versions later than August 1993.)

Complete listings of the CTH input decks used for the simulations are given in Appendices A-F. If the only difference in the input decks was the penetrator striking velocity, conservation method, or whether or not the BLINT model with or without the strength correction factor was used, then those decks are not listed. Notes in the input decks describe the required changes needed for the input decks not listed.

3. Results and Discussion

Initial impact conditions and ballistic test results [6] from the experiments are provided in Table 2 and simulation results are provided in Appendix G. The total penetrator yaw in the experiments was small (in most cases less than 1°). However, these values still exceed the critical yaw as defined in Bjerke et al. [23, 24] since the penetration channel diameter is about the same as the penetrator shank diameter for rigid body penetration of soft targets (e.g., see Forrestal et al. [25]). Any effects of yaw were not treated in the simulations.

In the following discussion, simulations will be designated by the options used. The designation will be of the form XX-XX-XX-X, where the first set of X's represents whether or not KE or MV was conserved during the convection phase of a computational cycle, the second set of X's represents whether the BLINT model was used (BL) or not used (NB), the third set of X's represents whether the yield strength correction factor was used with the BLINT model (CO) or not used (NC),

Table 2. Initial Impact Conditions and Ballistic Test Results

Shot No.	Total Yaw (o)	Striking Velocity (m/s)	Original Mass (g)	Residual Velocity (m/s)	Comments
Hemi-Nose Penetrators vs. 7.62-cm-Thick 7039 Aluminum					
4326	0.56	1,198	65.2	1,020	Eroded
4327	0.71	1,038	65.2	964	Rigid?
4328	0.71	1,093	65.5	961	Bulge, Fractured
Hemi-Nose Penetrators vs. 7.62-cm-Thick 5083 Aluminum					
4329	0.25	1,283	65.7	1,168	Eroded
4330	0.35	1,201	65.7	1,109	Slight Bulge
4331	0.25	1,147	65.8	1,069	Rigid, Fractured
Ogival-Nose Penetrators vs. 7.62-cm-Thick 5083 Aluminum					
4332	0.25	1,286	63.2	1,245	Rigid
4333	0.56	1,399	63.5	1,352	Rigid
4334	0.35	1,534	63.5	1,493	Rigid
4335	0.00	1,600	63.6	1,562	Rigid
Ogival-Nose Penetrators vs. 7.62-cm-Thick 7039 Aluminum					
4336	1.03	1,474	63.3	1,414	Rigid, Fractured
4337	0.56	1,595	63.5	1,528	Rigid, Fractured
4451	0.00	1,755	~63.5	1,677	Slight Bulge
4452	0.79	1,768	~63.5	1,652	Eroded, Bent

and the final X represents whether the threshold pressure failure model was used (P) or the strain-based failure model was used (S). For example, the designation KE-BL-CO-P Sim would mean that this simulation conserved KE during the convection phase of a computational cycle, that the BLINT model was used with the strength correction factor, and that the threshold pressure was used to model failure. The designations KE-BL-CO-P and MV-BL-CO-P represent the baseline simulations and will for simplicity also be called KE Sim(s) or MV Sim(s), respectively.

3.1 Residual Shapes for Baseline Simulations. Figure 2 compares the hemi-nose penetrator shapes predicted by the KE and MV Sims with tracings of residual penetrator shapes obtained from radiographs of the experiments against the 5083 aluminum targets. While the simulation results are all to the same scale and can be directly compared to their initial geometry (Figure 2a), the experimental penetrator shapes may not be at the same scale. The effective plastic strains in the penetrator for the simulations are also shown with strains less than 5% not being plotted. Visible deformation of the penetrator occurs when plastic strains between 45 and 55% (represented by green) appear on axis of the penetrator. The tracings show that the experimental hemi-nose penetrator remained rigid (although its tail fractured) at a striking velocity of 1,147 m/s (Figure 2b). At a striking velocity of 1,201 m/s, the onset of plastic deformation of the nose was observed (Figure 2c), and at a striking velocity of 1,283 m/s, the penetrator was significantly eroded (Figure 2d). The condition of the hemi-nose penetrator predicted by the KE Sim of the 1,147-m/s test was also rigid, although the fracture of the tail observed experimentally did not occur (Figure 2b). Erosion of the penetrator is evident in the KE Sim for the striking velocity of 1,201 m/s (Figure 2c). At a striking velocity of 1,283 m/s, the residual penetrator predicted by the KE Sim shows about the same amount of nose deformation and rod length as in the experiment (Figure 2d). For the MV Sims, the hemi-nose penetrator also remains rigid at a striking velocity of 1,147 m/s (Figure 2b). At striking velocities of 1,201 m/s and 1,283 m/s (Figures 2c and 2d), the MV Sims displayed much less plastic deformation and erosion of the rod nose than the experiments or the KE Sims.

The final hemi-nose penetrator shapes from both the experiments and the baseline simulations for the 7039 aluminum targets are shown in Figure 3. The apparent yaw seen in the figure for the experiments is not representative of any yaw the penetrator may have experienced in the experiments. Experimentally, the hemi-nose penetrators fractured at the two lower velocities tested (Figures 3b and 3c). At a striking velocity of 1,038 m/s it is unclear whether the penetrator in the experiment remained rigid (Figure 3b). Erosion, plastic deformation, and bending of the penetrator are evident at a striking velocity of 1,093 m/s (Figure 3c). At a striking velocity of 1,198 m/s, the eroded penetrator shows a sizable bulge at the nose as well as yaw into or out of the page (Figure 3d). The penetrator in the KE Sims remained essentially rigid at a striking velocity of 1,038 m/s (Figure 3b). Plastic deformation occurred at a striking velocity of 1,093 m/s (as seen by

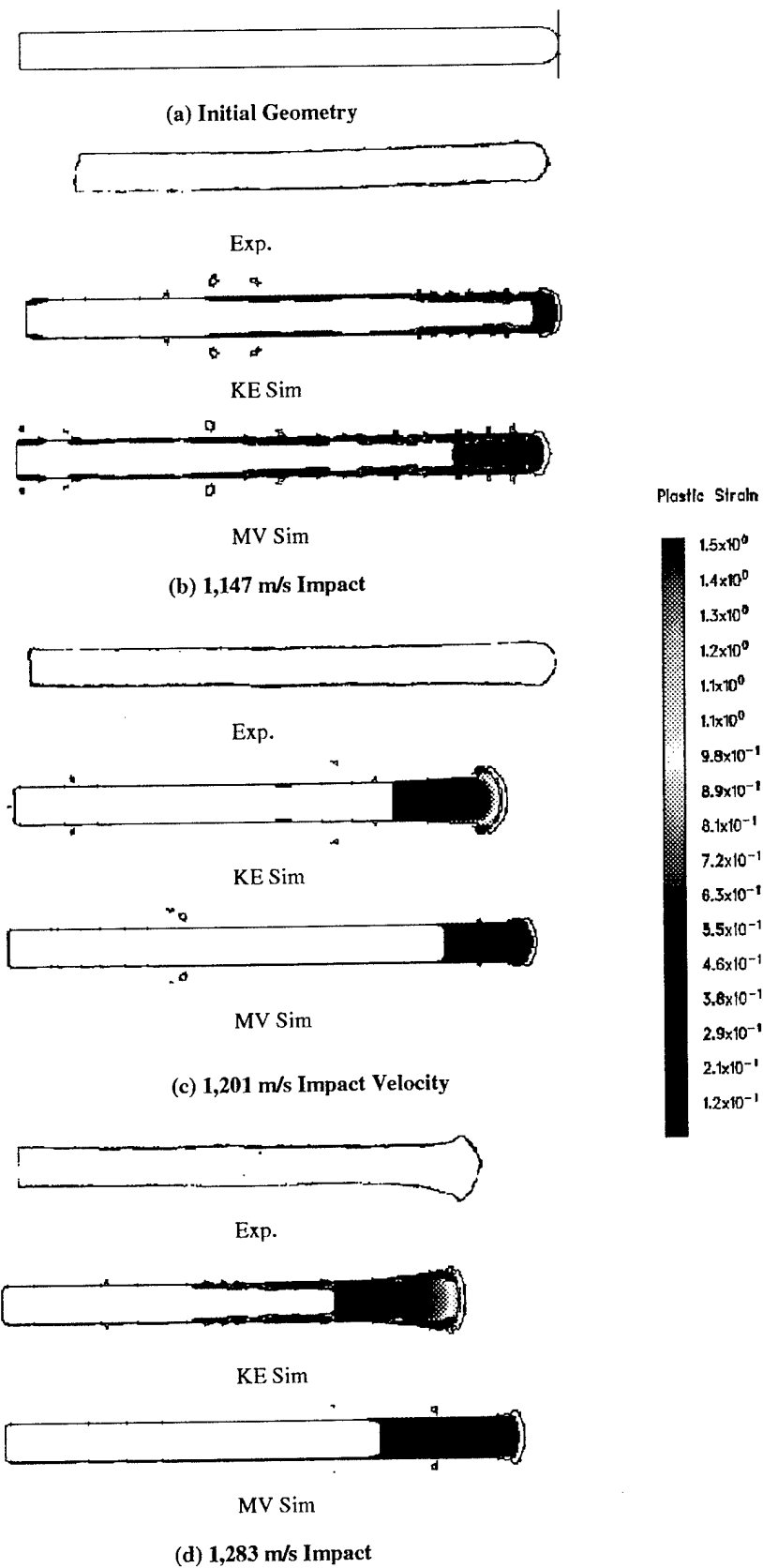


Figure 2. Comparison of Hemi-Nose Penetrator KE and MV Sims Residual Shapes With Experiment After Perforating 5083 Aluminum Targets.

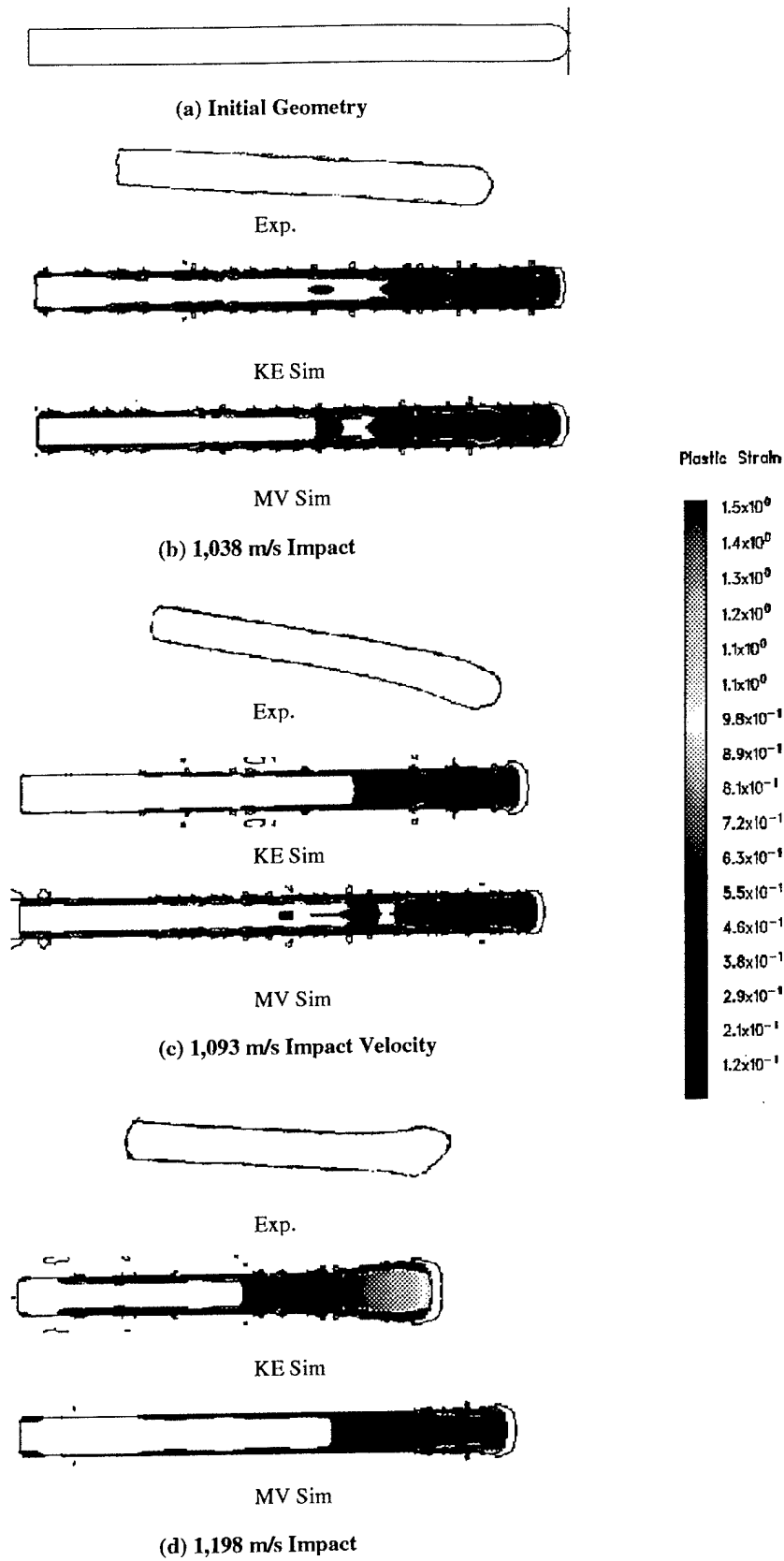


Figure 3. Comparison of Hemi-Nose Penetrator KE and MV Sims Residual Shapes With Experiment After Perforating 7039 Aluminum Targets.

the green color in the nose in Figure 3c). A large bulge and erosion in the penetrator are evident at a striking velocity of 1,198 m/s (Figure 3d). For the MV Sims, the penetrator also remains rigid at a striking velocity of 1,038 m/s (Figure 3b). The predicted length and shape of the penetrator at a striking velocity of 1,093 m/s were about the same as they had been at a striking velocity of 1,038 m/s (Figure 3c). The penetrator is clearly deformed at a striking velocity of 1,198 m/s as seen from plastic strains in the green range at the axis in the nose of the penetrator (Figure 3d).

Because the KE Sims and hemi-nose options seem to predict the onset of visible deformation and predict rod shape better than the MV Sims, most additional simulations were all modeled with the KE convection conservation option. Results for the ogival-nose penetrator MV Sims will be presented only at striking velocities for which experimental data were available at the time of the original paper [8]; therefore, no additional MV Sims will be presented. Predictions of the ogival-nose penetrator's threshold velocity were completed in advance of the experiments. Because it was felt that the threshold velocity of the ogival-nose penetrator may exceed the experimental gun system's maximum launch velocity and because of funding constraints, experiments were not completed for the 5083 aluminum target.

Figures 4 and 5 show the residual shapes and plastic strains for the ogival-nose penetrator after perforating 5083 aluminum targets for the KE and MV Sims, respectively. The experimental penetrator shapes are not shown because they remain rigid at all striking velocities tested (see Table 2). It can be seen from Figure 4 that the amount of plastic stain experienced by the penetrators increased with striking velocity. Not until the penetrator experienced plastic strain between 46 and 55% (beginning of the green range) on the penetrator axis can one see significant difference in the residual shape of the penetrator (Figure 4h). From Figure 4, it is clearly evident that visible plastic deformation occurs at striking velocities between 1,900 and 2,000 m/s for the KE Sims. At a striking velocity of 2,100 m/s, the KE Sim ogival-nose penetrator is clearly eroded (Figure 4i). The MV Sim ogival-nose penetrators of Figure 5 seem to experience larger plastic strain at the same corresponding striking velocity than do their KE Sim counterparts (Figure 4).

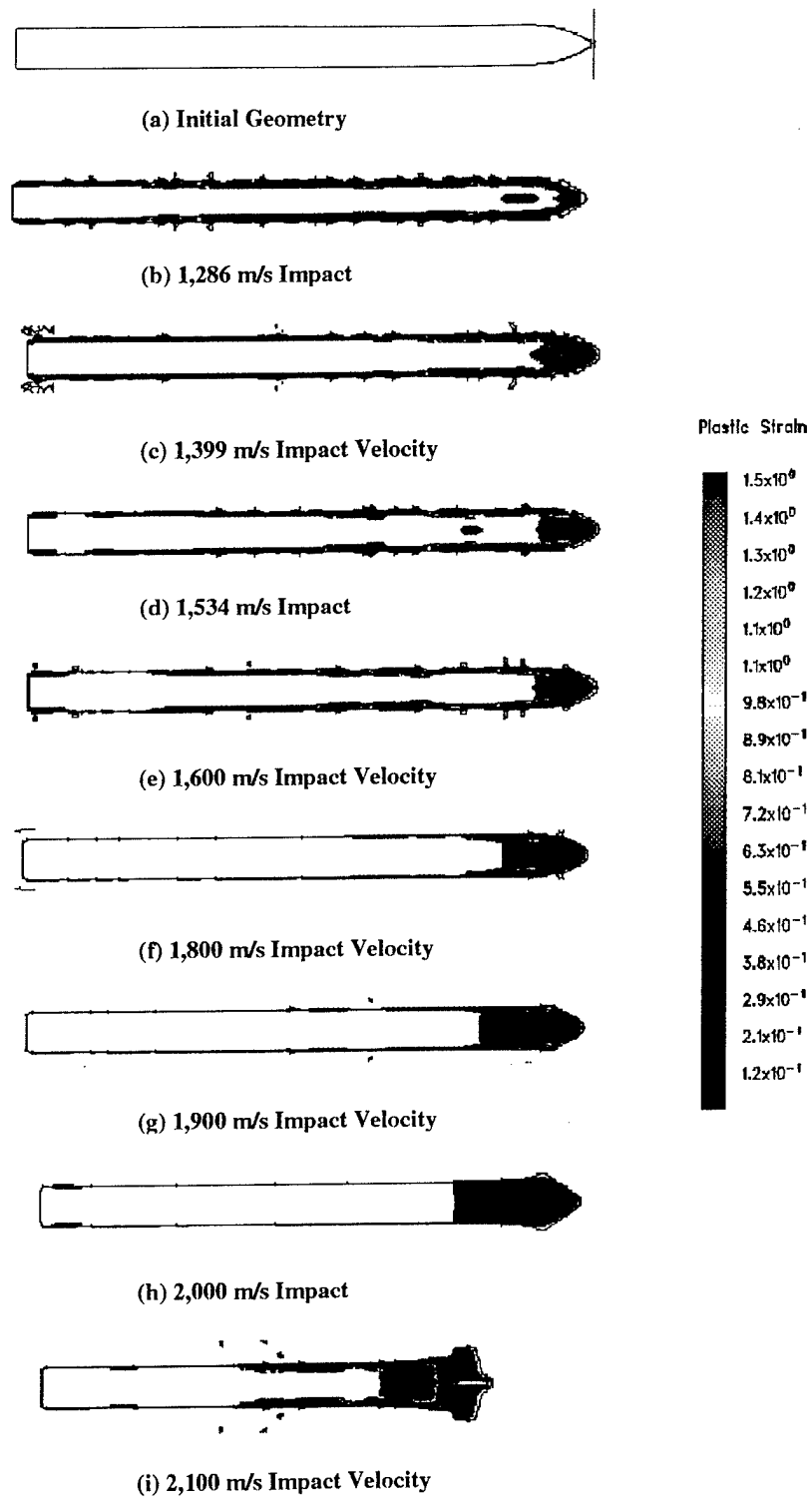


Figure 4. Residual Shapes of the Ogival-Nose Penetrator KE Sims After Perforating 5083 Aluminum Targets.

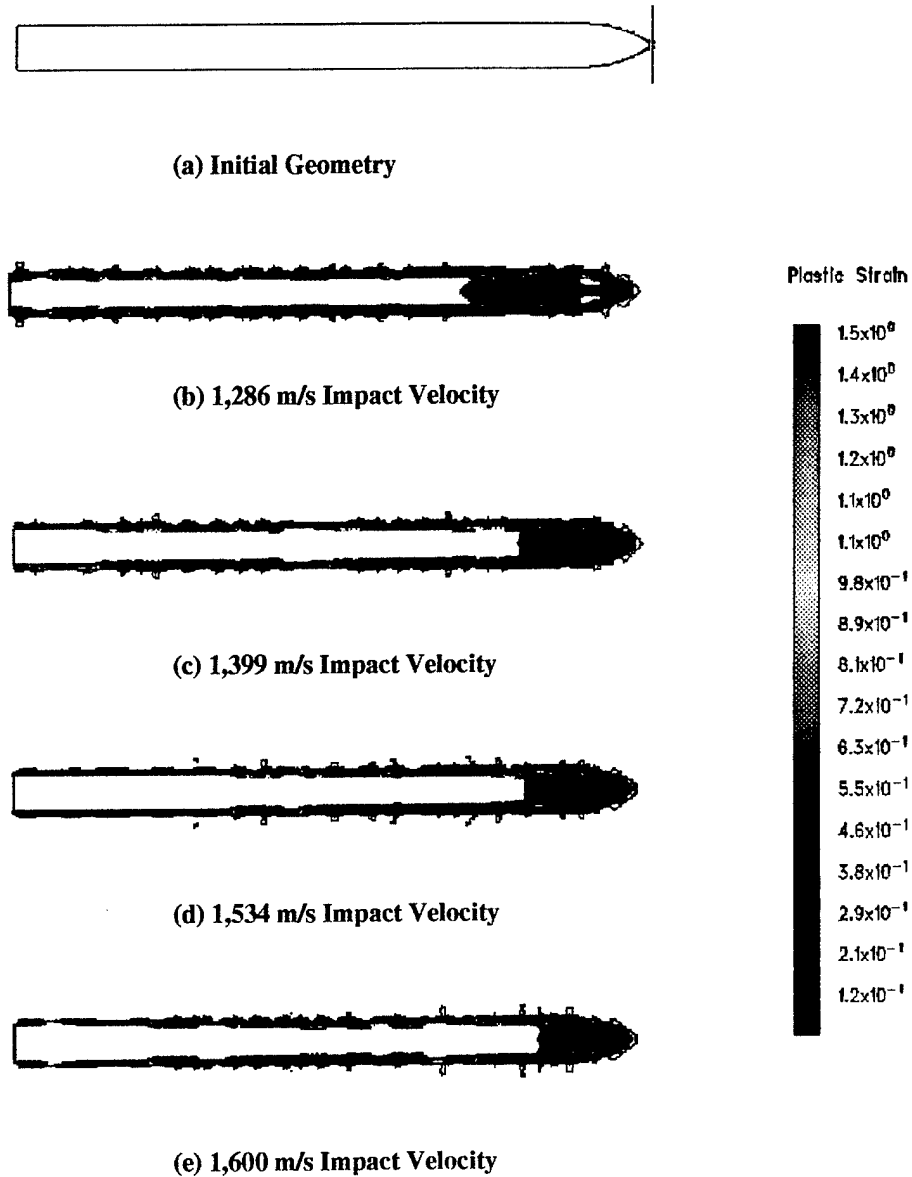
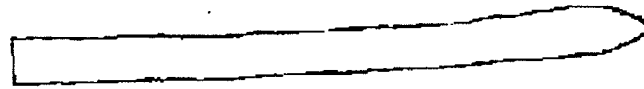
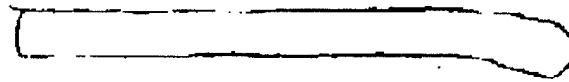


Figure 5. Residual Shapes of the Ogival-Nose Penetrator MV Sims After Perforating 5083 Aluminum Targets.

Figures 6, 7, and 8 show the residual shapes for the ogival-nose penetrator impacting 7039 aluminum targets from the experiments, KE Sims and MV Sims, respectively. For the experiments, only two shapes are shown at the striking velocities between which the transition from rigid-body penetration to eroding rod occurred. These two experiments were conducted after the simulations were completed. Residual shapes of lower velocity ogival-nose penetrator experiments are not shown as they all remain rigid. In the experiments, plastic deformation and bending of the penetrator



(a) 1,755 m/s Impact Velocity



(b) 1,768 m/s Impact Velocity

Figure 6. Experimentally Determined Residual Shapes of the Ogival-Nose Penetrator After Perforating 7039 Aluminum Targets.

are evident for a striking velocity of 1,755 (Figure 6a). With an increase in striking velocity of 13 m/s, the penetrator is clearly eroded (Figure 6b), suggesting that the transition velocity lies between a striking velocity of 1,755 and 1,768 m/s. The KE Sims predicted that the onset of plastic deformation occurred between a striking velocity of 1,800 and 1,900 m/s (Figures 7d and 7e) and that erosion occurred between a striking velocity of 1,900 and 2000 m/s. Again the MV Sims seem to show much larger plastic strains at the corresponding striking velocity than do the KE Sims (Figures 7 and 8).

3.2 Residual Velocity for Baseline Simulations. Figure 9 compares the predicted residual velocity of the penetrators to the experimentally determined residual velocity for the 5083 aluminum targets. The experimental results are represented with solid symbols, the KE Sims are represented with hollow symbols, and the MV Sims are represented with half-filled symbols. In addition, the hemi-nose penetrators are represented by circles and the ogival-nose penetrators are represented by squares. In all cases, the predicted residual velocities are less than the experimentally determined ones. Not much difference is seen in the predicted residual velocities of the ogival-nose penetrator, though the KE Sims show a slight improvement over the MV Sims. Most ogival-nose predictions were within 8.1% of the experimentally determined residual velocities with the exception being the MV Sim at a striking velocity of 1,286 m/s, which differed by 13.1%. For the hemi-nose penetrators,

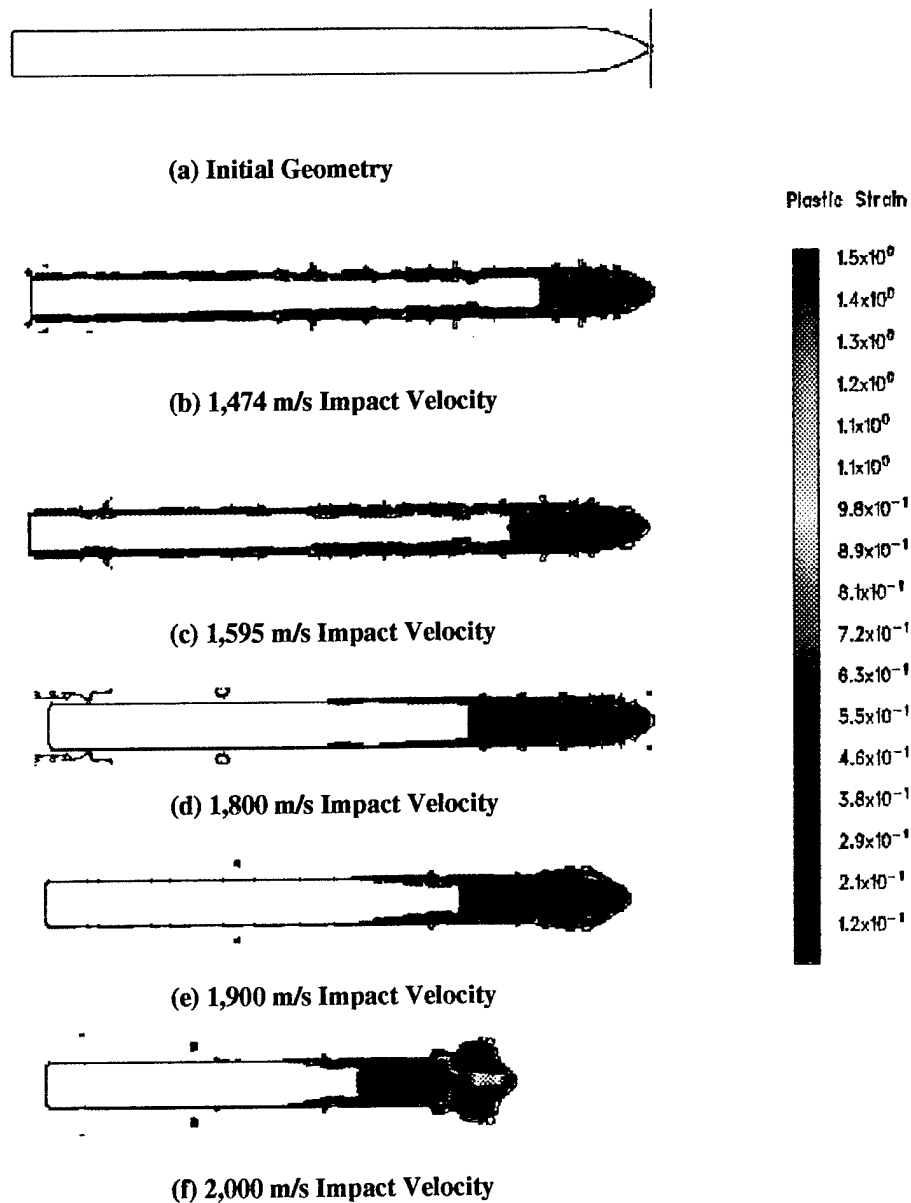


Figure 7. Residual Shapes of the Ogival-Nose Penetrator KE Sims After Perforating 7039 Aluminum Targets.

the predicted residual velocities for the simulations were much better for the MV Sims than for the KE Sims, except for the datum at the lowest striking velocity. In general, the difference between the predicted and the experimentally determined residual velocities for the hemi-nose penetrators was less than 7.4% for KE Sims and less than 2.3% for MV Sims, except for the datum at the lowest striking velocity, which differed by 9.0%.

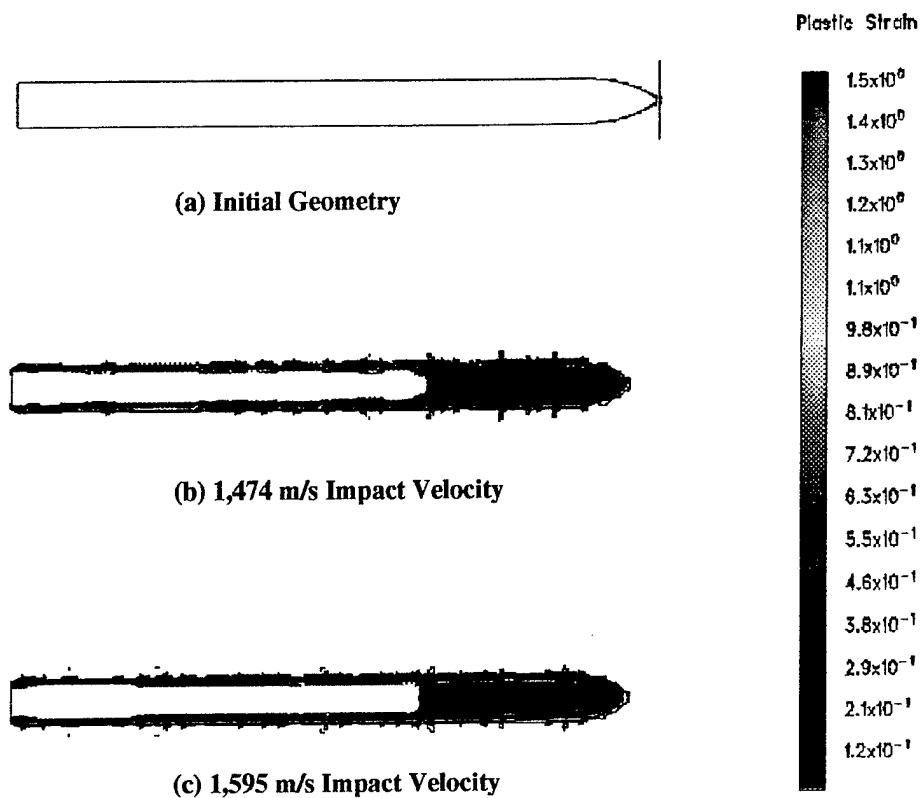


Figure 8. Residual Shapes of the Ogival-Nose Penetrator MV Sims After Perforating 7039 Aluminum Targets.

Figure 10 compares the experimental residual velocity data with the baseline simulations' predicted residual velocity for the 7039 aluminum targets. The symbols are the same as were used in Figure 10 for the 5083 aluminum target. Again, the CTH hydrocode's predicted residual velocities are less than those obtained experimentally for all cases considered. The predicted residual velocities for the ogival-nose penetrator were within 8.4% of those obtained experimentally, with only a slight difference in the predictions between the KE and MV Sims. The fact that the hemi-nose penetrator experiments show almost identical residual velocities for the striking velocities of 1,038 m/s and 1,093 m/s suggests a transition from rigid body penetrator to eroding/deforming penetration between these two velocities. The hemi-nose KE Sims show near identical residual velocities for striking velocities of 1,093 m/s and 1,198 m/s suggesting that the transition velocity lies between these two velocities. For the MV Sims, it is not clear from looking at the residual velocities whether a transition from rigid body to eroding rod penetration took place. The predicted

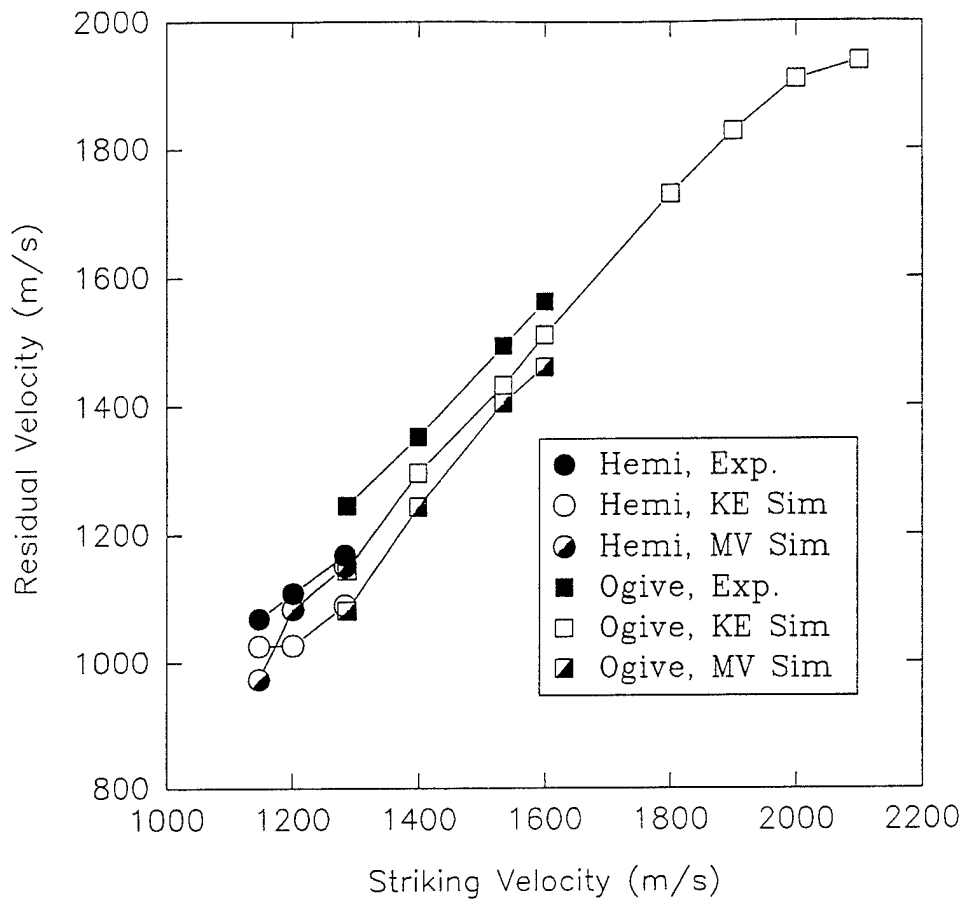


Figure 9. Residual Velocity Comparison Between Experiment, KE, and MV Sims After Perforating 5083 Aluminum Targets.

residual velocities for the KE Sims are closer to the experimentally determined residual velocities than are the MV Sims, for all but one datum.

3.3 BLINT Model Parameters. To show the differences that using the BLINT model can make in predictions, three of the KE Sims for the 5083 aluminum targets were repeated without the BLINT model active (KE-NB-NC-P Sims). The repeated simulations include the hemi-nose penetrator shown in Figure 2b (which remained rigid), the hemi-nose penetrator shown in Figure 2d (which was visibly deformed/eroded), and the ogival-nose penetrator at the highest velocity tested (Figure 5e, which remained rigid). Figure 11 shows the predicted shapes of the three KE Sims that were repeated without the BLINT model active. The hemi-nose penetrator that was previously predicted to remain rigid (Figure 2b) is now excessively deformed (Figure 11a). The hemi-nose penetrator that

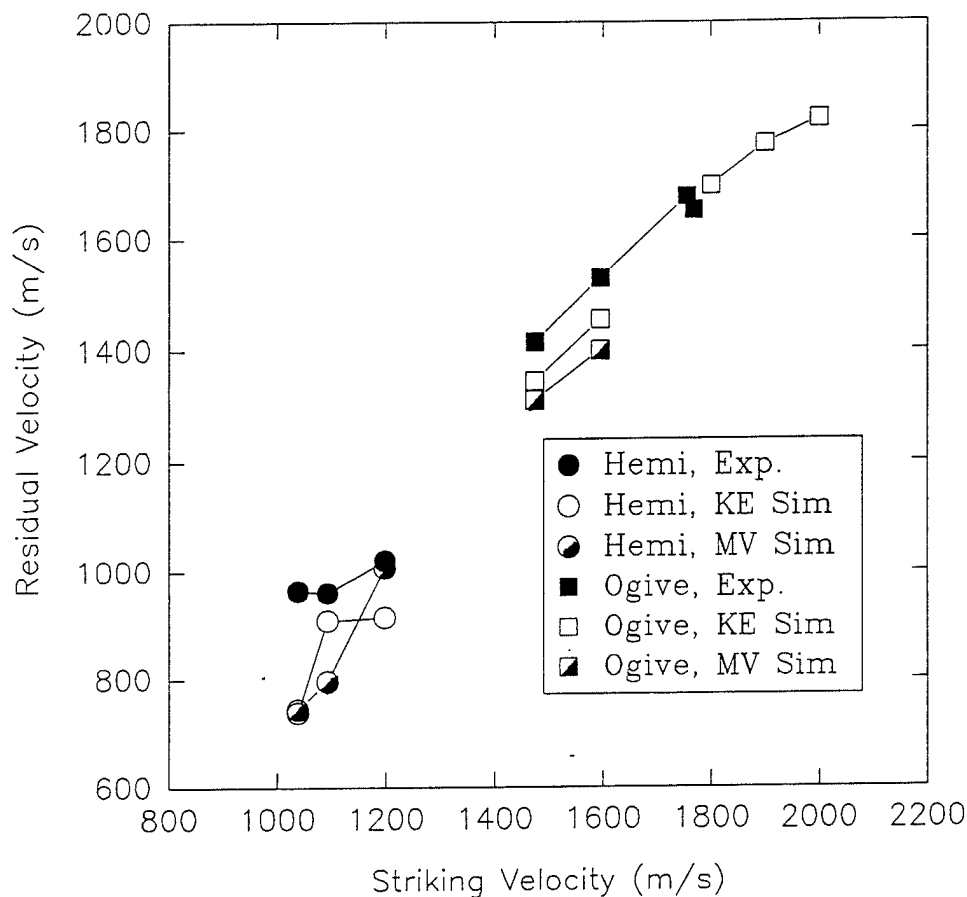


Figure 10. Residual Velocity Comparison Between Experiment, KE, and MV Sims After Perforating 7039 Aluminum Targets.

was previously predicted to erode (Figure 2b) is now predicted to deform and erode excessively (Figure 11b). Finally, with the BLINT model active, all the ogival-nose penetrators were predicted to remain rigid at all striking velocities simulated; however, without the BLINT model, erosion is predicted (Figure 11c). Figure 12 compares the residual velocities of the KE Sims with and without the BLINT model to the experimentally determined values. In all cases, the predicted residual velocities for the KE-NB-NC-P Sims underpredicted those with the BLINT model active. The degree to which the KE-NB-NC-P Sims underpredicted experiment seems to increase at the lower initial striking velocities.

To examine the effect the yield strength correction factor has on simulation results, the hemi- and ogival-nose KE Sims against the 5083 aluminum target were repeated without the strength correction

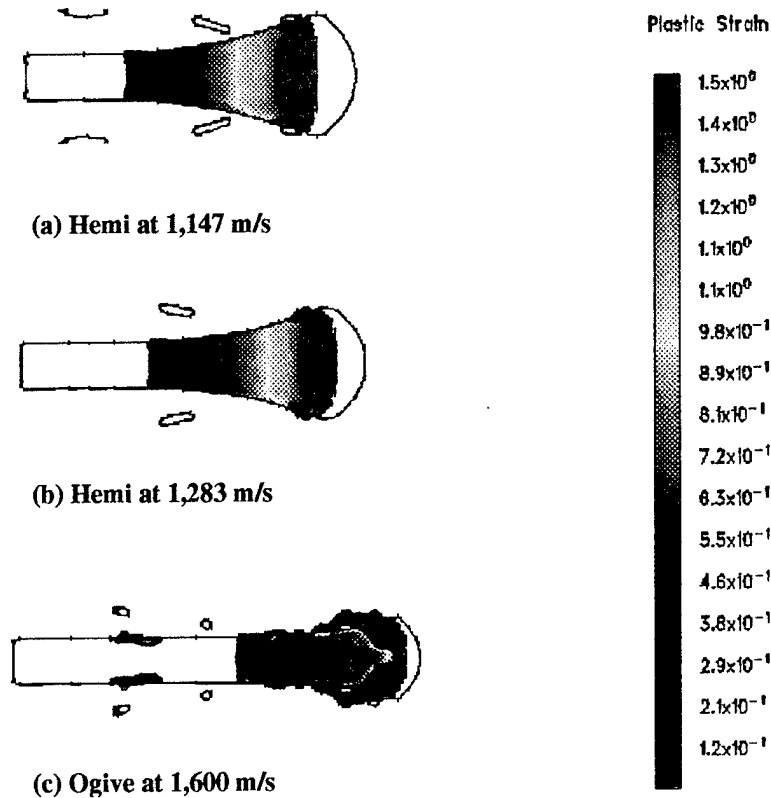


Figure 11. Residual Shapes of KE-NB-NC-P Sims After Perforating 5083 Aluminum Targets.

factor (KE-BL-NC-P Sims). Residual shapes and plastic strains of the hemi- and ogival-nose penetrators are shown in Figures 13 and 14, respectively. The hemi-nose KE-BL-NC-P Sims (Figure 13) appear to deform in a manner similar to the hemi-nose KE-NB-NC-P Sims (Figures 11a and 11b). The baseline KE Sims for the ogival-nose penetrators shown in Figures 4b–4e remained rigid. Without the strength correction factor, the ogival-nose penetrator shows visible deformation at the very tip of the nose at a striking velocity of 1,286 m/s (Figure 14b) that progressively increases with striking velocity (Figures 14c–14e). The residual velocity for the KE-BL-NC-P Sims is compared to the experimental results and the KE-BL-CO-P baseline simulations in Figure 15. The KE-BL-NC-P Sims underpredict the experimental determined residual velocity to a greater extent than the baseline KE Sims. At striking velocities of 1,286 m/s and 1,399 m/s, the predicted residual

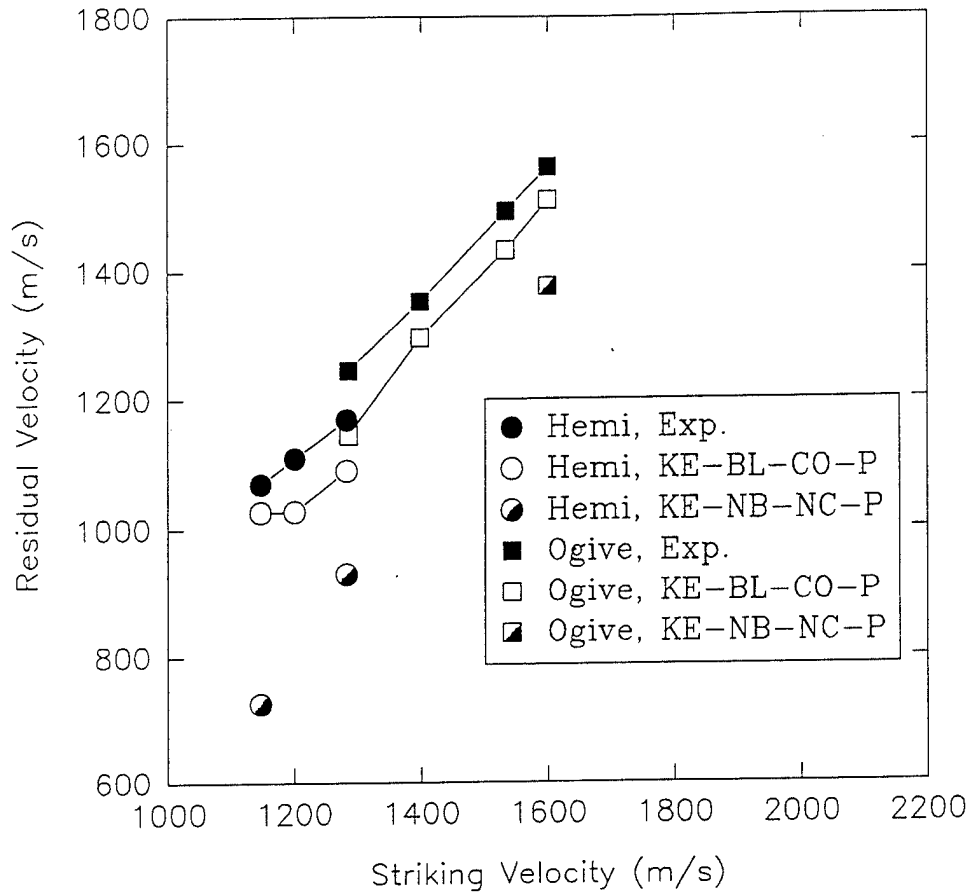


Figure 12. Comparison of Residual Velocity for KE-NB-NC-P Sims With Experiment and Baseline KE Sims After Perforating 5083 Aluminum Targets.

velocities for the ogival-nose penetrator are close to the baseline predictions, because the penetrator was only slightly deformed (Figures 14b and 14c).

3.4 Failure Model Effects. In examining the effects of nose shape on the threshold velocity at which tungsten alloy penetrators transition from rigid body to eroding rods when penetrating deep aluminum targets, it has been shown that the failure model used can influence the predicted penetration depth [8, 9]. Magness has suggested a more appropriate failure model would be one based on strain [26], the reasons for which are given in Magness [27]. Therefore, all KE Sims for the 5083 aluminum targets using the BLINT model were redone using the Johnson-Cook failure with all but the first parameter set to zero, such that all materials would fail when they exceeded a threshold value of 150% strain or when they exceeded the threshold value of tensile pressure

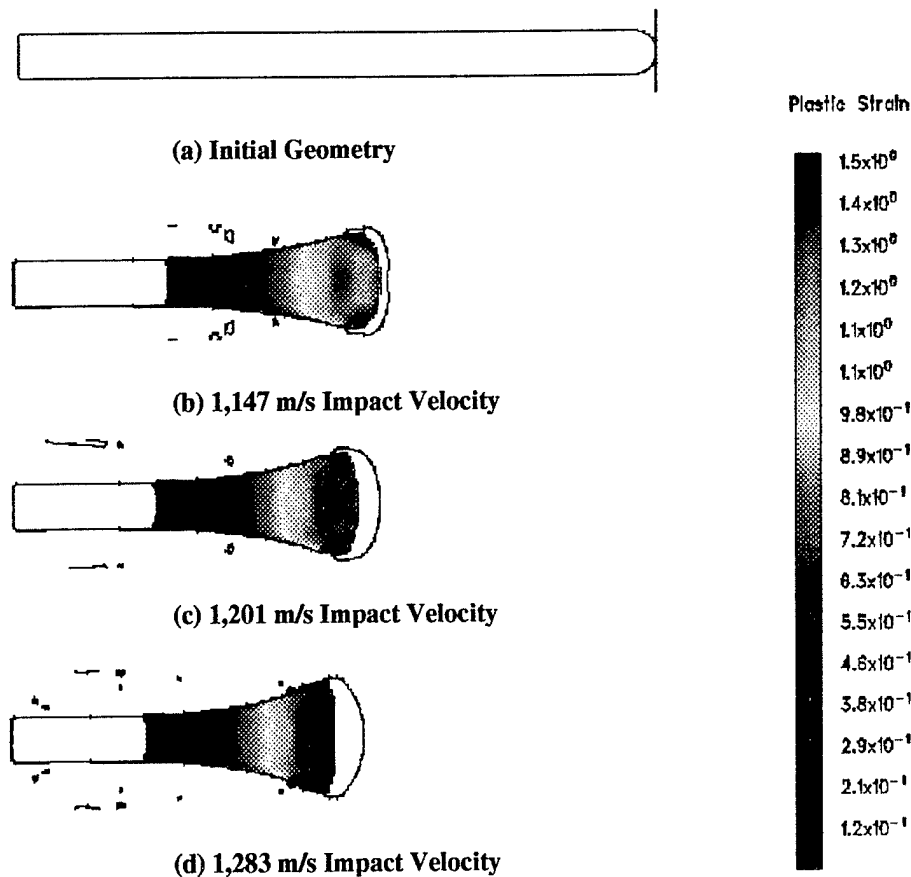


Figure 13. Residual Shapes for Hemi-Nose Penetrator KE-BL-NC-P Sims After Perforating 5083 Aluminum Targets.

reported earlier. The predicted shapes for the KE-BL-CO-S hemi-nose penetrators (Figure 16) do not differ significantly from the baseline KE Sims (Figures 2b–2d), and the predicted threshold velocity remains the same (between 1,147 and 1,201 m/s). Even the levels of effective plastic strain observed are similar. The KE-BL-CO-S ogival-nose penetrators (Figure 17) remained rigid for all striking velocities considered as did the baseline KE Sim counterparts (Figures 4b–4e); however the KE-BL-CO-S experienced larger plastic strains for the same striking velocity. Using a strain-based failure criteria reduced the predicted residual velocity for all simulations when compared to the baseline KE Sims and experimental results other than for the hemi-nose penetrator with a striking velocity of 1,201 m/s (Figure 18).

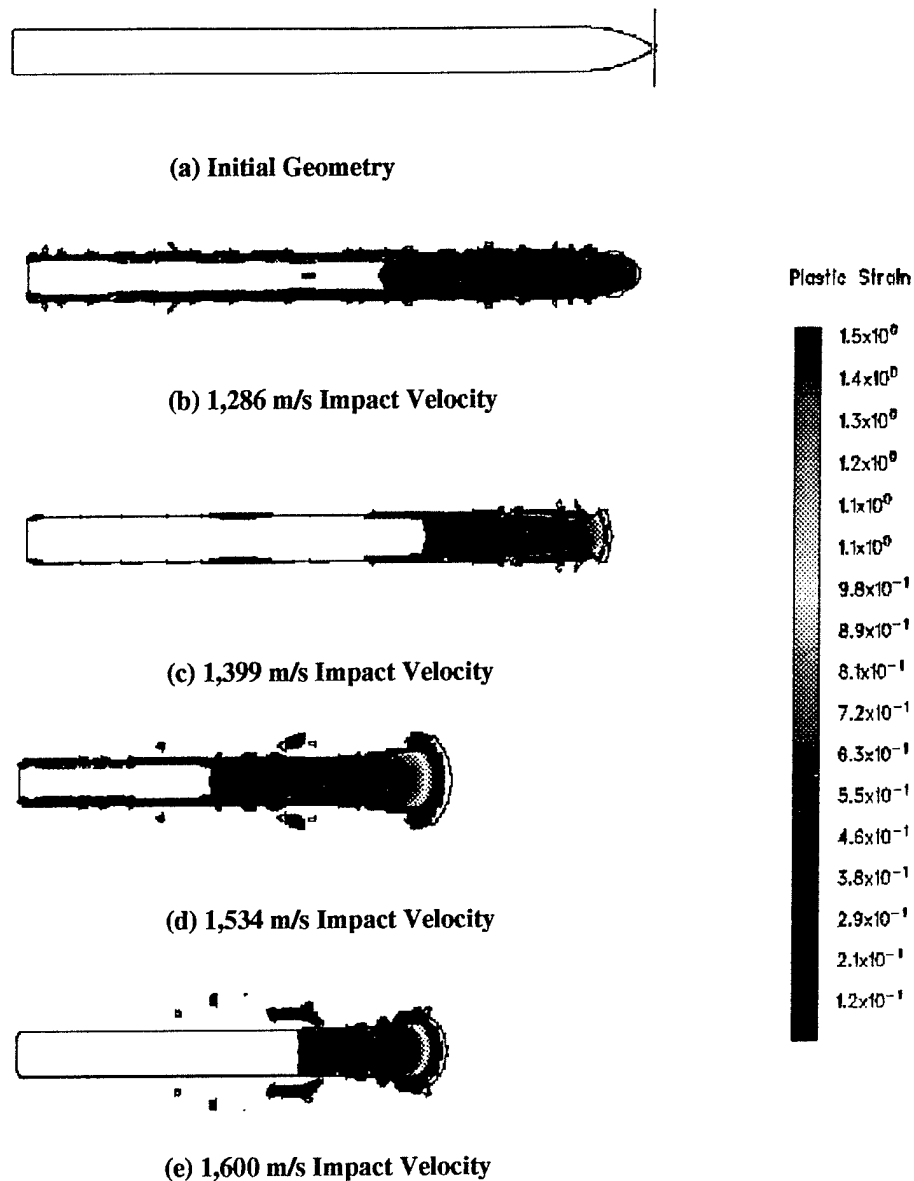


Figure 14. Residual Shapes for Ogival-Nose Penetrator KE-BL-NC-P Sims After Perforating 5083 Aluminum Targets.

4. Conclusions

It is known that the constitutive response of tungsten alloy is dependent on strain, strain rate, temperature, percentage tungsten content, tungsten grain size, and amount of swaging [28]. In addition, for solid-solid impacts at velocities of 500–2,000 m/s, impact pressures rapidly decay to values comparable to the strength of the material; therefore, the constitutive model is of primary

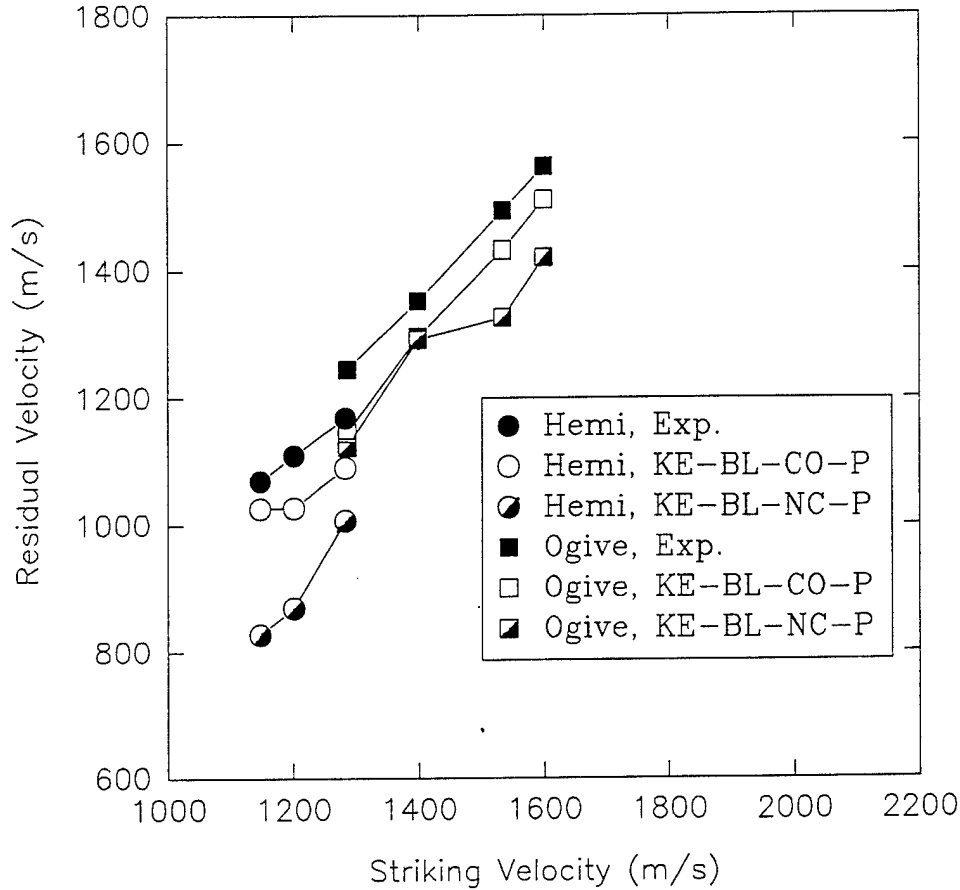


Figure 15. Comparison of Residual Velocity for KE-BL-NC-P Sims With Experiment and Baseline KE Sims After Perforating 5083 Aluminum Targets.

importance and the EOS is of secondary importance [29]. Therefore, it is unrealistic to expect the results of the simulations, with the constitutive model approximations used for the 95W-2.5Ni-1.0Fe-1.5Co, 21% swaged alloy, to provide an exact match with the experimental data. Nevertheless, the following conclusions are offered.

The BLINT model represents a drastic improvement in the predictive capabilities in the CTH hydrocode for certain types of penetration scenarios, such as rigid body penetrations. The hydrocode was able to predict the effect of rod nose-shape on the threshold velocity at which transition from rigid body to eroding rod penetration occurs. The code successfully estimated the velocity at which the hemi-nose penetrators begin to deform in penetrating either 5083 or 7039 aluminum. The transition occurs at a much higher striking velocity for an ogival-nose penetrator than for a hemi-

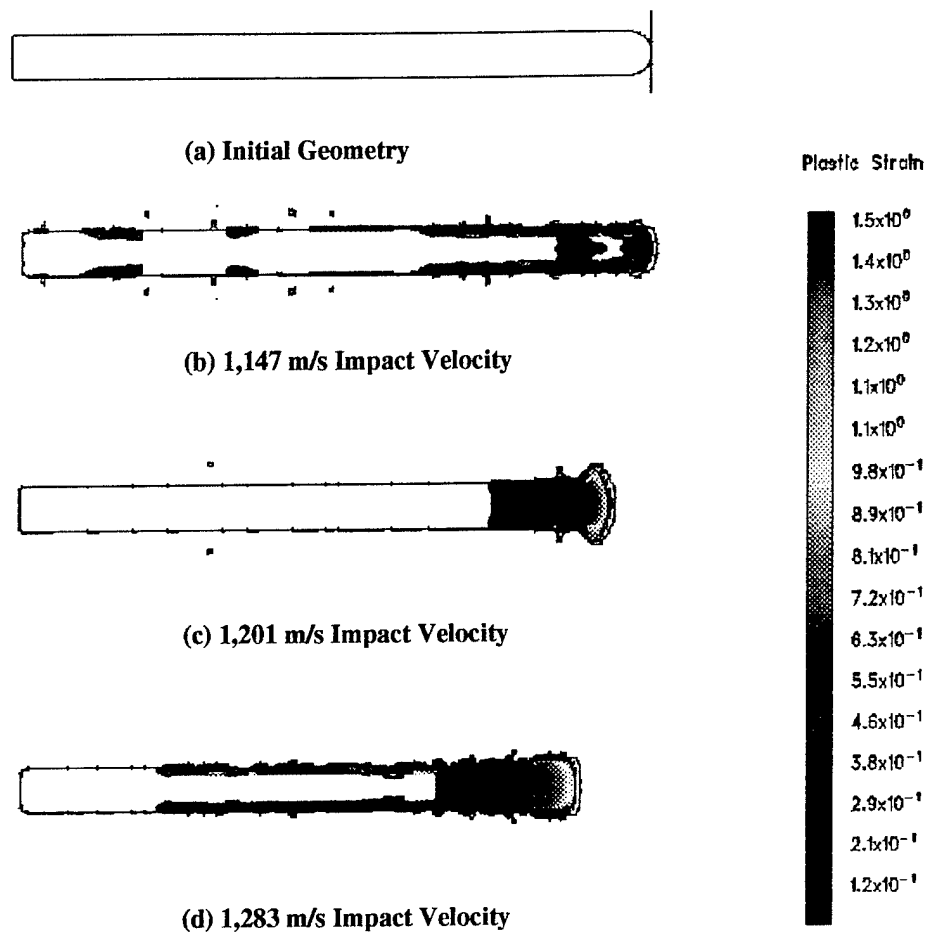


Figure 16. Residual Shapes for Hemi-Nose Penetrator KE-BL-CO-S Sims After Perforating 5083 Aluminum Targets.

nose penetrator. Experimentally, the transition occurred with the onset of plastic deformation of the hemi-nose penetrator at a striking velocity of 1,201 m/s to full erosion at a striking velocity of 1,283 m/s when impacting a 5083 aluminum target. The KE Sims predicted the transition velocity for the hemi-nose penetrator would occur between a striking velocity of 1,147 and 1,201 m/s for the 5083 aluminum target. The MV Sims hemi-nose penetrator only predicted minimal plastic deformation in the range of striking velocities between 1,147 and 1,283 m/s for the 5083 aluminum target. Experimentally, the transition velocity for the ogival-nose penetrator impacting the 5083 aluminum target was never determined. The KE Sims predicted the visible plastic deformation would occur at a striking velocity between 1,900 and 2,000 m/s and erosion of the penetrator would

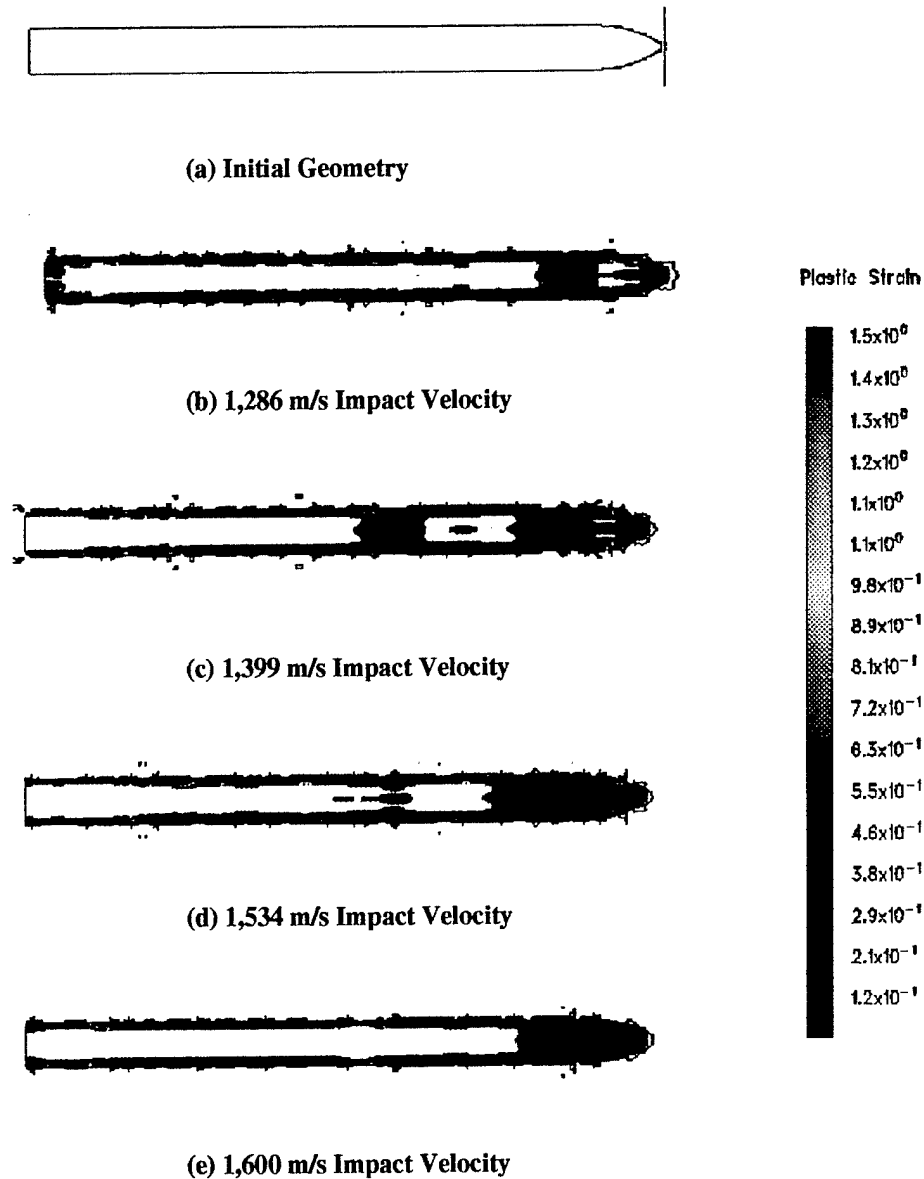


Figure 17. Residual Shapes for Ogival-Nose Penetrator KE-BL-CO-S Sims After Perforating 5083 Aluminum Targets.

occur at a striking velocity between 2,000 and 2,100 m/s for the ogival-nose penetrator impacting a 5083 aluminum target. The transition velocity was not determined for the ogival-nose MV Sims.

Experimentally, for the hemi-nose penetrator impacting a 7039 aluminum target, plastic deformation occurred between a striking velocity of 1,038 and 1,093 m/s and erosion occurred between a striking velocity of 1,093 and 1,198 m/s. The same result was predicted by the hemi-nose

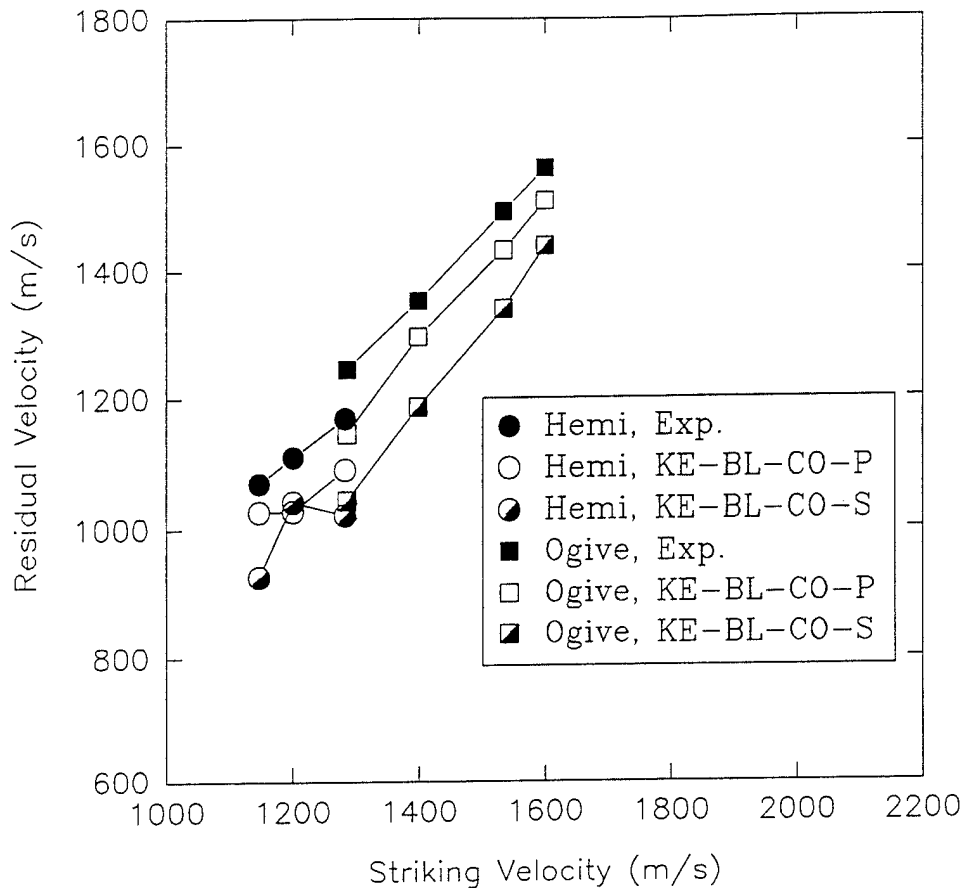


Figure 18. Comparison of Residual Velocity for KE-BL-CO-S Sims With Experiment and Baseline KE Sims After Perforating 5083 Aluminum Targets.

KE Sims for the 7039 aluminum target. The MV Sims predicted visible plastic deformation would occur between a striking velocity of 1,093 and 1,198 m/s for a 7039 aluminum target. Experimentally, the transition velocity occurred between a striking velocity of 1,755 and 1,768 m/s for the ogival-nose penetrator impacting a 7039 aluminum target. The ogival-nose KE Sims predicted visible plastic deformation would occur at a striking velocity between 1,800 and 1,900 m/s and erosion at a striking velocity between 1,900 and 2,000 m/s when impacting a 7039 aluminum target.

While the simulations were not in complete agreement with experiment, they did a reasonable job at predicting the transition velocities and did an excellent job predicting all the experimental trends. The simulations predicted the large difference in the transition velocity for a hemi-nose and

ogival-nose penetrator, and they correctly predicted the effect of target materials. In general, the baseline KE Sims did much better at predicting final rod shape than did the MV Sims.

The baseline KE Sims did better in predicting residual velocity than did the MV Sims for both target materials. Both the ogival-nose KE and MV Sims were within 8.1% of the experimentally determined residual velocity, except for one datum. The hemi-nose MV Sims were closer to predicting the experimentally determined residual velocity for the 5083 aluminum target, and the KE Sims were closer to predicting the experimentally determined residual velocity for the 7039 aluminum target. For the 5083 aluminum target, the hemi-nose KE and MV Sims predicted the residual velocity within 9%. For the 7039 aluminum target, the hemi-nose KE and MV Sims under predicted residual velocity by as much as 24%.

It has been shown that without the BLINT model CTH cannot accurately model transition velocity or the perforation of finite target plates. Hemi- and ogival-nose penetrators that were previously predicted to remain rigid, eroded and deformed excessively without the BLINT model active. A hemi-nose penetrator previously predicted to erode, eroded and deformed excessively. Due to excessive deformation predicted with the BLINT model inactive, the predicted residual velocities were significantly underpredicted. It was also shown that the yield strength correction factor greatly influenced simulation results. Without the yield strength correction factor, hemi-nose penetrator simulation results were similar to those without the BLINT model active. Without the yield strength correction factor, the ogival-nose penetrators deformed and eroded prematurely. As a result, most simulations run without the yield strength correction factor under predicted residual velocity by a significant amount.

Finally, it was shown that the choice of material failure models could influence simulation results. The residual shapes and residual velocities predicted using a strain-based failure model did not differ significantly for the hemi-nose simulations. The predicted residual velocity was greatly influenced by the choice of failure models. No attempt was made to predict the transition velocity for ogival-nose simulations using a strain-based failure model. However, the effective plastic strains in the ogival-nose penetrators were greater than the baseline simulations, suggesting that the

transition velocity might be lower. The residual velocities predicted by the ogival-nose penetrator using a strain-based failure model were somewhat reduced.

5. References

1. McGlaun, J. M., S. L. Thompson, and M. G. Elrick. "CTH: A Three-Dimensional Shock Wave Physics Code." *International Journal of Impact Engineering*, vol. 10, no. 1-4, pp. 351-360, 1990.
2. Zukas, J. A. Memorandum, U.S. Army Research Laboratory, Aberdeen Proving Ground, MD, 1991.
3. Silling, S. A. "CTH Reference Manual: Boundary Layer Algorithm for Sliding Interfaces in Two Dimensions." SAND93-2487, Sandia National Laboratories, Albuquerque, NM, 1994.
4. Silling, S. A. "Eulerian Simulation of the Perforation of Aluminum Plates by Nondeforming Projectiles." SAND92-0493, Sandia National Laboratories, Albuquerque, NM, 1992.
5. Kmetyk, L. N., and P. Yarrington. "CTH Analyses of Steel Rod Penetration Into Aluminum and Concrete Targets With Comparisons to Experimental Data." SAND94-1498, Sandia National Laboratories, Albuquerque, NM, 1994.
6. Magness, L. S., Jr. U.S. Army Research Laboratory, Aberdeen Proving Ground, MD, unpublished data.
7. Scheffler, D. R. "CTH Hydrocode Simulations of Hemispherical and Ogival Nose Tungsten Alloy Penetrators Perforating Finite Aluminum Targets." PVP-Vol. 325 (edited by Y. S. Shin and J. A. Zukas), *Structures Under Extreme Loading Conditions*, New York: ASME, pp. 125-136, 1996.
8. Scheffler, D. R. "CTH Hydrocode Predictions on the Effect of Rod Nose-Shape on the Velocity at Which Tungsten Alloy Rods Transition From Rigid Body to Eroding Penetrators When Impacting Thick Aluminum Targets." *Structures Under Shock and Impact IV* (edited by N. Jones, C. A. Brebbia, and A. J. Watson), pp. 297-310, *Proceedings of the Fourth International Conference On Structures Under Shock and Impact (SUSI96)*, Udine, Italy, 3-5 July 1996, Computational Mechanics Publications, Ashurst Lodge, Southampton, UK, 1996.
9. Scheffler, D. R. "Modeling the Effect of Penetrator Nose-Shape on Threshold Velocity for Thick Aluminum Targets." ARL-TR-1417, U.S. Army Research Laboratory, Aberdeen Proving Ground, MD, July 1997.
10. Johnson, G. R., and W. H. Cook. "A Constitutive Model and Data Subjected to Large Strains, High Strain Rates and High Temperatures." *Proceedings of the Seventh International Symposium on Ballistics*, The Hague, The Netherlands, pp. 541-548, 1983.

11. Zerilli, F. J., and R. W. Armstrong. "Dislocation-Mechanics-Based Constitutive Relations for Material Dynamics Calculations." *Journal of Applied Physics*, vol. 61, no. 5, pp. 1816–1825, 1987.
12. Steinberg, D. J., S. G. Cochran, and M. W. Guinan. "A Constitutive Model for Metals Applicable at High-Strain Rate." *Journal of Applied Physics*, vol. 51, no. 3, pp. 1498–1504, 1980.
13. Steinberg, D. J., and C. M. Lund. "A Constitutive Model for Strain Rates From 10^{-4} to 10^6 s^{-1} ." *Journal of Applied Physics*, vol. 65, no. 4, pp. 1528–1533, 1989.
14. Kerley, G. I. "CTH Equation of State Package: Porosity and Reactive Burn Models." SAND92-0553, Sandia National Laboratories, Albuquerque, NM, 1992.
15. Lee, E. L., H. C. Hornig, and J. W. Kury. "Adiabatic Expansion of High Explosive Detonation Products." UCRL-50422, Lawrence Livermore National Laboratory, Livermore, CA, 1968.
16. Johnson, G. R., and W. H. Cook. "Fracture Characteristics of Three Metals Subjected to Various Strains, Strain Rates, Temperatures, and Pressures." *Journal of Engineering Fracture Mechanics*, vol. 21, no. 1, pp. 31–48, 1985.
17. Noh, W. F., and P. Woodward. "SLIC (Simple Line Interface Calculation)." *Lecture Notes in Physics*, vol. 59, New York: Springer-Verlag, 1976.
18. Bell, R. L., and E. S. Hertel Jr. "An Improved Material Interface Reconstruction Algorithm for Eulerian Codes." SAND92-1716, Sandia National Laboratories, Albuquerque, NM, 1992.
19. Steinberg, D. J. "Equation of State and Strength Properties of Selected Materials." UCRL-MA-106439, Lawrence Livermore National Laboratory, Livermore, CA, 1991.
20. Forrestal, M. J., V. K. Luk, and N. S. Brar. "Perforation of Aluminum Armor Plates With Conical-Nose Projectiles." *Mechanics of Materials*, vol. 10, nos. 1–2, pp. 97–105, 1990.
21. Boyer, H. E., and T. L. Gall (eds.). *Metals Handbook Desk Edition*, American Society for Metals, OH, 1985.
22. Bell, R. L., M. G. Elrick, E. S. Hertel Jr., G. I. Kerley, L. N. Kmetyk, J. M. McGlaun, J. S. Rottler, S. A. Silling, P. A. Taylor, S. L. Thompson, L. Yarrington, and F. J. Zeigler. "CTH User's Manual and Input Instructions Version 1.027." Sandia National Laboratories, Albuquerque, NM, 1993.
23. Bjerke, T. W., G. F. Silsby, D. R. Scheffler, and R. M. Mudd. "Yawed Long Rod Armor Penetration at Ordnance and Higher Velocities." BRL-TR-3221, U.S. Army Ballistic Research Laboratory, Aberdeen Proving Ground, MD, 1991.

24. Bjerke, T. W., G. F. Silsby, D. R. Scheffler, and R. M. Mudd. "Yawed Long-Rod Armor Penetration." *International Journal of Impact Engineering*, vol. 12, no. 2, pp. 281-292, 1992.
25. Forrestal, M. J., D. Y. Tzou, E. Askari, and D. B. Longscope. "Penetration Into Ductile Metal Targets With Rigid Spherical-Nose Rods." *International Journal of Impact Engineering*, vol. 16, nos. 5-6, pp. 699-710, 1995.
26. Magness, L. S., Jr. Private communication. U.S. Army Research Laboratory, Aberdeen Proving Ground, MD, 1995.
27. Magness, L. S., Jr. "Properties and Performance of KE Penetrator Materials." Tungsten & Tungsten Alloys-1992 (edited by A. Brose and R. J. Dowding), pp. 15-22, *Proceedings of the International Conference on Tungsten & Tungsten Alloys*, Arlington, VA, 1992, Metal Powder Industries Federation, Princeton, NJ, 1993.
28. Coates, R. S., and K. T. Ramesh. "The Deformation of Tungsten Alloys at High Strain Rates." Shock-Wave and High-Strain-Rate Phenomena in Materials (edited by M. A. Meyers, L. E. Murr, and K. P. Staudhammer), pp. 203-212, *Proceeding of the International Conference on the Material Effects of Shock-Wave and High-Strain-Rate Phenomena*, San Diego, CA, 1990, New York: Marcel Dekker, Inc., 1992.
29. Zukas, J. A., T. Nicholas, H. F. Swift, L. B. Greszczuk, and D. R. Curran. *Impact Dynamics*. New York: Wiley-Interscience, 1982.

INTENTIONALLY LEFT BLANK.

Appendix A:

**Input for Hemi-Nose KE-BL-CO-P Sims vs. 5083 Aluminum
Targets - Changes for MV, NB, and NC Sims Given in Notes**

INTENTIONALLY LEFT BLANK.

```

* Run History
*
*eor* cgenin
*
nose shape tests: hemi v=1147 target=5083 al finite
*
control
ep
mmp
viscosity bl=.1 bq=2 bs=0.1
endcontrol
*
mesh
block 1 geom=2dc type=e
x0 0.00
x1 n 40 w 1.6891 rat 1.0
x2 n 45 dxf 0.0422275 rat 1.05
endx
y0 -10.219055
y1 n 832 dyf 0.0422275 rat 1.0
endy
xactive 0.0 0.4
yactive -10.219055 0.0
endblock
endmesh
*
insertion
block 1
package '5083 Al target'
material 1
numsub 50
insert box
p1=0.0 0.0
p2=7.6 7.62
endinsert
endpackage
package 'w alloy rod nose'
material 2
numsub 100
*
* NOTE: striking velocity (yvel) is changed below
*
yvel 1.147e5
insert circle
ce=0.0 -0.33782

```

```

    r= 0.33782
    endinsert
    endpackage
    package 'w alloy rod body'
    material 2
    numsub 50
*
* NOTE: striking velocity (yvel) is changed below
*
    yvel 1.147e5
    insert box
    p1=0.0 -0.33782
    p2=0.33782 -10.1346
    endinsert
    endpackage
    endblock
endinsertion
*
epdata
vpsave
*
* NOTE: poisson ratio from Tungsten from Metals Handbook, that for 5083
*       Aluminum from Forrestal, M.J., V. K. Luk, and N. S. Brar, "Perforation of
*       aluminum with conical-nose projectiles", Mechanic and Materials 10 (1990)
*       pp. 97-105.
*
* NOTE: properties for 5083 aluminum from Silling, S. A., "CTH Reference Manual:
*       Boundary Layer Algorithm for Sliding Interfaces in Two Dimensions", Sandia
*       National Laboratories Report SAND93-2487, January 1994.
*
* NOTE: 5083 aluminum using undocumented power law
*
    matep 1
    johnson-cook='USER'
        ajo=-2.76e9 bjo=254.7 cjo=0.0
        mjo=1.0 njo=0.084 tjo=6.68e-2
        poisson 0.333
*
* NOTE: actual tungsten alloy was 95W-2.5Ni-1.0Fe-1.5Co (21% swaged) with r0=18.1.
*       95W-3.5Ni-1.5Fe is being used to approximate the w alloy.
*
    matep 2
    steinberg='TUNGSTEN_NI_FE'
        r0st=18.16 tm0st=0.195002 atmst=1.3
        gm0st=1.67 ast=1.03e-12 bst=1.76396

```

```

nst=0.13  c1st=0.0  c2st=0.0
g0st=1.45e12 btst=7.7  eist=0.0
ypst=0.0  ukst=0.0  ysmst=0.0
yast=0.0  y0st=18.7e9  ymst=40.e9
poisson=0.280
*
* NOTE: parameters for boundary layer algorithm taken similar to:
*       Kmetyk, L. N. and P. Yarrington, "CTH Analysis of Steel Rod Penetration
*       Into Aluminum and Concrete Targets with Comparisons to Experimental Data",
*       Sandia National Laboratories Report SAND94-1498, October 1994.
*
* NOTE: if no BLINT model, next line is commented out. If no yield strength correction
*       factor 'corr' is omitted
*
      blint 1 soft 1 hard 2 wsl 0.084455 wbl 0.084455 fric=0.0 corr
      mix 3
endep
*
tracer
  block 1
    add 0. 0. to 0. -10.134 n 10
endtracer
*
edit
  block 1
    noexpanded
  endblock
endedit
*
eos
*
* NOTE: EOS properties from cth mgrun library
*
* NOTE: 5083-H131 Aluminum eos approximated with 6061-t6 Aluminum
*       density reduced to reflect that for 5083 Aluminum from
*       Metal's Handbook.
*
      mat1 mgrun eos=6061-t6_al r0=2.66  cs=0.534e6  s=1.4
              g0=1.97  cv=1.07e11
      mat2 mgrun eos=tungsten_ni r0=18.16  cs=0.403e6  s=1.237
              g0=1.67  cv=1.66e10
endeos
*
*cor* cthin
*
```

```

nose shape tests: hemi v=1147 target=5083 al finite
*
control
  tstop 300.e-6
  rdumpf 3600
  cpshift 999.
endcontrol
*
restart
* file='rsct1'
  time=0.e-6
endr
*
cellthermo
  mmp
  ntbad=99999
endc
*
convct
*
* NOTE: if KE Sim convection=0, if MV Sim convection=1
*
  convection=0
  interface=high_resolution
endconvct
*
edit
  shortt
    time 0. dtfrequency 150.e-6
  ends
  longt
    time 0. dtfrequency 600.e-6
  endl
  plott
    time 0. dtfrequency 50.e-6
  endp
  histt
    time 0. dtfrequency 0.3e-6
  htracer1
  htracer2
  htracer3
  htracer4
  htracer5
  htracer6
  htracer7

```

```

    htracer8
    htracer9
    htracer10
endh
ende
*
boundary
  bhydro
    block 1
      bxbot 0
      bxtop 2
      bybot 2
      bytop 2
    endb
  endh
endb
*
fracts
  pressure
  pfrac1 -4.5e9
  pfrac2 -35.0e9
  pfmix -1.0e20
  pfvoid -1.0e20
endf
*
*eor* pltinp
*
```

INTENTIONALLY LEFT BLANK.

Appendix B:

**Input for Ogival-Nose KE-BL-CO-P Sims vs. 5083 Aluminum
Targets - Changes for MV, NB, and NC Sims Given in Notes**

INTENTIONALLY LEFT BLANK.

```

** Run History
*
*eor* cgenin
*
nose shape tests: ogive v=1286 target=5083 al finite
*
control
  ep
  mmp
  viscosity bl=.1 bq=2 bs=0.1
endcontrol
*
mesh
  block 1 geom=2dc type=e
    x0 0.00
    x1 n 40 w 1.6891 rat 1.0
    x2 n 45 dxf 0.0422275 rat 1.05
  endx
  y0 -10.219055
  y1 n 832 dyf 0.0422275 rat 1.0
  endy
  xactive 0.0 0.4
  yactive -10.219055 0.0
endblock
endmesh
*
insertion
  block 1
    package '5083 Al target'
    material 1
    numsub 50
    insert box
      p1=0.0 0.0
      p2=7.6 7.62
    endinsert
  endpackage
  package 'w alloy ogive nose rod'
  material 2
  numsub 100
*
* NOTE: striking velocity (yvel) is changed below
*
  yvel 1.286e5
  insert uds
    point 0.0 0.0

```

```

point 0.050437038 -0.08003015622
point 0.095867718 -0.1600603124
point 0.136665799 -0.2400904687
point 0.173135779 -0.3201206249
point 0.205527612 -0.4001507811
point 0.234047376 -0.4801809373
point 0.258865148 -0.5602110935
point 0.280120900 -0.6402412498
point 0.297928948 -0.7202714060
point 0.312381319 -0.8003015622
point 0.323550306 -0.8803317184
point 0.331490355 -0.9603618746
point 0.336239443 -1.040392031
point 0.337820 -1.120422187
point 0.337820 -10.1346
point 0.0 -10.1346
point 0.0 0.0
endinsert
endpackage
endblock
endinsertion
*
epdata
vpsave
*
* NOTE: poisson ratio from for Tungsten from Metals Handbook, that for 5083
* Aluminum from Forrestal, M.J., V. K. Luk, and N. S. Brar, "Perforation of
* aluminum with conical-nose projectiles", Mechanic and Materials 10 (1990)
* pp. 97-105.
*
* NOTE: properties for 5083 aluminum from Silling, S. A., "CTH Reference Manual:
* Boundary Layer Algorithm for Sliding Interfaces in Two Dimensions", Sandia
* National Laboratories Report SAND93-2487, January 1994.
*
* NOTE: 5083 aluminum using undocumented power law
*
matep 1
johnson-cook='USER'
      ajo=-2.76e9 bjo=254.7 cjo=0.0
      mjo=1.0 njo=0.084 tjo=6.68e-2
      poisson 0.333
*
* NOTE: actual tungsten alloy was 95W-2.5Ni-1.0Fe-1.5Co (21% swaged) with r0=18.1.
* 95W-3.5Ni-1.5Fe is being used to approximate the w alloy.
*

```

```

matep 2
  steinberg='TUNGSTEN_NI_FE'
    r0st=18.16  tm0st=0.195002  atmst=1.3
    gm0st=1.67  ast=1.03e-12  bst=1.76396
    nst=0.13  c1st=0.0  c2st=0.0
    g0st=1.45e12  btst=7.7  eist=0.0
    ypst=0.0  ukst=0.0  ysmst=0.0
    yast=0.0  y0st=18.7e9  ymst=40.e9
    poisson=0.280
*
* NOTE: parameters for boundary layer algorithm taken similar to:
*       Kmetyk, L. N. and P. Yarrington, "CTH Analysis of Steel Rod Penetration
*       Into Aluminum and Concrete Targets with Comparisons to Experimental Data",
*       Sandia National Laboratories Report SAND94-1498, October 1994.
*
* NOTE: if no BLINT model, next line is commented out. If no yield strength correction
*       factor 'corr' is omitted
*
  blint 1 soft 1 hard 2 wsl 0.084455 wbl 0.084455 fric=0.0 corr
  mix 3
endep
*
tracer
  block 1
  add 0. 0. to 0. -10.1345 n 10
endtracer
*
edit
  block 1
  noexpanded
endblock
endedit
*
eos
*
* NOTE: EOS properties from cth mgrun library
*
* NOTE: 5083-H131 Aluminum eos approximated with 6061-t6 Aluminum
*       density reduced to reflect that for 5083 Aluminum from
*       Metal's Handbook.
*
mat1 mgrun eos=6061-t6_al r0=2.66  cs=0.534e6  s=1.4
      g0=1.97  cv=1.07e11
mat2 mgrun eos=tungsten_ni r0=18.16  cs=0.403e6  s=1.237
      g0=1.67  cv=1.66e10

```

```

endeos
*
*eor* cthin
*
nose shape tests: ogive v=1286 target=5083 al finite
*
control
  tstop 300.e-6
  rdumpf 3600
  cpshift 999.
endcontrol
*
restart
* file='rsct1'
  time=0.e-6
endr
*
cellthermo
  mmp
  ntbad=99999
endc
*
convct
*
* NOTE: if KE Sim convection=0, if MV Sim convection=1
*
  convection=0
  interface=high_resolution
endconvct
*
edit
  shortt
    time 0. dtfrequency 150.e-6
  ends
  longt
    time 0. dtfrequency 600.e-6
  endl
  plott
    time 0. dtfrequency 50.e-6
  endp
  histt
    time 0. dtfrequency 0.3e-6
  htracer1
  htracer2
  htracer3

```

```

    htracer4
    htracer5
    htracer6
    htracer7
    htracer8
    htracer9
    htracer10
endh
ende
*
boundary
  bhydro
    block 1
      bxbot 0
      bxtop 2
      bybot 2
      bytop 2
    endb
  endh
endb
*
fracts
  pressure
  pfrac1 -4.5e9
  pfrac2 -35.0e9
  pfmix -1.0e20
  pfvoid -1.0e20
endf
*
*eor* pltinp
*
```

INTENTIONALLY LEFT BLANK.

Appendix C:

**Input for Hemi-Nose KE-BL-CO-P Sims vs. 7039 Aluminum
Targets - Changes for MV, NB, and NC Sims Given in Notes**

INTENTIONALLY LEFT BLANK.

```

* Run History
*
*eor* cgenin
*
nose shape tests: hemi v=1038 target=7039 al finite
*
control
  ep
  mmp
  viscosity bl=.1 bq=2 bs=0.1
endcontrol
*
mesh
  block 1 geom=2dc type=e
    x0 0.00
    x1 n 40 w 1.6891 rat 1.0
    x2 n 45 dxf 0.0422275 rat 1.05
  endx
  y0 -10.219055
  y1 n 832 dyf 0.0422275 rat 1.0
  endy
  xactive 0.0 0.4
  yactive -10.219055 0.0
endblock
endmesh
*
insertion
  block 1
    package '7039 Al target'
    material 1
    numsub 50
    insert box
      p1=0.0 0.0
      p2=7.6 7.62
    endinsert
  endpackage
  package 'w alloy rod nose'
  material 2
  numsub 100
*
* NOTE: striking velocity (yvel) is changed below
*
  yvel 1.038e5
  insert circle
    ce=0.0 -0.33782

```

```

    r= 0.33782
endinsert
endpackage
package 'w alloy rod body'
    material 2
    numsub 50
*
* NOTE: striking velocity (yvel) is changed below
*
    yvel 1.038e5
    insert box
        p1=0.0 -0.33782
        p2=0.33782 -10.1346
    endinsert
endpackage
endblock
endinsertion
*
epdata
vpsave
*
* NOTE: poisson's ratio from Metals Handbook
*
    matep 1
    johnson-cook='7039_ALUMINUM'
        ajo=3.3672e9 bjo=3.4293e9 cjo=0.01
        mjo=1.0 njo=.41 tjo=7.76342e-2
        poisson 0.345
*
* NOTE: actual tungsten alloy was 95W-2.5Ni-1.0Fe-1.5Co (21% swaged) with r0=18.1.
*       95W-3.5Ni-1.5Fe is being used to approximate the w alloy.
*
    matep 2
    steinberg='TUNGSTEN_NI_FE'
        r0st=18.16 tm0st=0.195002 atmst=1.3
        gm0st=1.67 ast=1.03e-12 bst=1.76396
        nst=0.13 c1st=0.0 c2st=0.0
        g0st=1.45e12 btst=7.7 eist=0.0
        ypst=0.0 ukst=0.0 ysmst=0.0
        yast=0.0 y0st=18.7e9 ymst=40.e9
        poisson=0.280
*
* NOTE: parameters for boundary layer algorithm taken similar to:
*       Kmetyk, L. N. and P. Yarrington, "CTH Analysis of Steel Rod Penetration
*       Into Aluminum and Concrete Targets with Comparisons to Experimental Data",

```

```

*      Sandia National Laboratories Report SAND94-1498, October 1994.
*
* NOTE: if no BLINT model, next line is commented out. If no yield strength correction
*       factor 'corr' is omitted
*
    blint 1 soft 1 hard 2 wsl 0.084455 wbl 0.084455 fric=0.0 corr
    mix 3
endep
*
tracer
    block 1
    add 0. 0. to 0. -10.134 n 10
endtracer
*
edit
    block 1
    noexpanded
endblock
endedit
*
eos
*
* NOTE: EOS properties from cth mgrun library
*
* NOTE: 7039 Aluminum eos approximated with 7075-t6 Aluminum
*       density reduced to reflect that for 7039 Aluminum from
*       Johnson and Cook (1983).
*
    mat1 mgrun eos=7075-t6_al r0=2.77  cs=0.520e6  s=1.36
           g0=2.20  cv=1.07e11
    mat2 mgrun eos=tungsten_ni r0=18.16 cs=0.403e6  s=1.237
           g0=1.67  cv=1.66e10
endeos
*
*eor* cthin
*
nose shape tests: hemi v=1038 target=7039 al finite
*
control
    tstop 300.e-6
    rdumpf 3600
    cpshift 999.
endcontrol
*
restart

```

```

* file='rsct1'
  time=0.e-6
endr
*
cellthermo
  mmp
  ntbad=99999
endc
*
convct
*
* NOTE: if KE Sim convection=0, if MV Sim convection=1
*
  convection=0
  interface=high_resolution
endconvct
*
edit
  shortt
    time 0. dtfrequency 150.e-6
  ends
  longt
    time 0. dtfrequency 600.e-6
  endl
  plott
    time 0. dtfrequency 50.e-6
  endp
  histt
    time 0. dtfrequency 0.3e-6
    htracer1
    htracer2
    htracer3
    htracer4
    htracer5
    htracer6
    htracer7
    htracer8
    htracer9
    htracer10
  endh
ende
*
boundary
  bhydro
  block 1

```

```
    bxbot 0
    bxtop 2
    bybot 2
    bytop 2
  endb
endh
endb
*
fracts
  pressure
  pfrac1 -5.0e9
  pfrac2 -35.0e9
  pfmix -1.0e20
  pfvoid -1.0e20
endf
*
*eor* pltinp
*
```

INTENTIONALLY LEFT BLANK.

Appendix D:

**Input for Ogival-Nose KE-BL-CO-P Sims vs. 7039 Aluminum
Targets - Changes for MV, NB, and NC Sims Given in Notes**

INTENTIONALLY LEFT BLANK.

* Run History

*

eor cgenin

*

nose shape tests: ogive v=1474 target=7039 al finite

*

control

ep

mmp

viscosity bl=.1 bq=2 bs=0.1

endcontrol

*

mesh

block 1 geom=2dc type=e

x0 0.00

x1 n 40 w 1.6891 rat 1.0

x2 n 45 dxf 0.0422275 rat 1.05

endx

y0 -10.219055

y1 n 832 dyf 0.0422275 rat 1.0

endy

xactive 0.0 0.4

yactive -10.219055 0.0

endblock

endmesh

*

insertion

block 1

package '7039 Al target'

material 1

numsub 50

insert box

p1=0.0 0.0

p2=7.6 7.62

endinsert

endpackage

package 'ogive nose rod'

material 2

numsub 100

*

* NOTE: striking velocity (yvel) is changed below

*

yvel 1.474e5

insert uds

point 0.0 0.0

```

point 0.050437038 -0.08003015622
point 0.095867718 -0.1600603124
point 0.136665799 -0.2400904687
point 0.173135779 -0.3201206249
point 0.205527612 -0.4001507811
point 0.234047376 -0.4801809373
point 0.258865148 -0.5602110935
point 0.280120900 -0.6402412498
point 0.297928948 -0.7202714060
point 0.312381319 -0.8003015622
point 0.323550306 -0.8803317184
point 0.331490355 -0.9603618746
point 0.336239443 -1.040392031
point 0.337820 -1.120422187
point 0.337820 -10.1346
point 0.0 -10.1346
point 0.0 0.0
endinsert
endpackage
endblock
endinsertion
*
epdata
vpsave
*
* NOTE: poisson's ratio from Metals Handbook
*
matep 1
johnson-cook='7039_ALUMINUM'
ajo=3.3672e9 bjo=3.4293e9 cjo=0.01
mjo=1.0 njo=.41 tjo=7.76342e-2
poisson 0.345
*
* NOTE: actual tungsten alloy was 95W-2.5Ni-1.0Fe-1.5Co (21% swaged) with r0=18.1.
* 95W-3.5Ni-1.5Fe is being used to approximate the w alloy.
*
matep 2
steinberg= 'TUNGSTEN_NI_FE'
r0st=18.16 tm0st=0.195002 atmst=1.3
gm0st=1.67 ast=1.03e-12 bst=1.76396
nst=0.13 clst=0.0 c2st=0.0
g0st=1.45e12 btst=7.7 eist=0.0
ypst=0.0 ukst=0.0 ysmst=0.0
yast=0.0 y0st=18.7e9 ymst=40.e9
poisson=0.280

```

```

*
* NOTE: parameters for boundary layer algorithm taken similar to:
*       Kmetyk, L. N. and P. Yarrington, "CTH Analysis of Steel Rod Penetration
*       Into Aluminum and Concrete Targets with Comparisons to Experimental Data",
*       Sandia National Laboratories Report SAND94-1498, October 1994.
*
* NOTE: if no BLINT model, next line is commented out. If no yield strength correction
*       factor 'corr' is omitted
*
    blint 1 soft 1 hard 2 wsl 0.084455 wbl 0.084455 fric=0.0 corr
    mix 3
endep
*
tracer
    block 1
    add 0. 0. to 0. -10.1345 n 10
endtracer
*
edit
    block 1
    noexpanded
endblock
endedit
*
eos
*
* NOTE: EOS properties from cth mgrun library
*
* NOTE: 7039 Aluminum eos approximated with 7075-t6 Aluminum
*       density reduced to reflect that for 7039 Aluminum from
*       Johnson and Cook (1983).
*
    mat1 mgrun eos=7075-t6_al r0=2.77 cs=0.520e6 s=1.36
           g0=2.20 cv=1.07e11
    mat2 mgrun eos=tungsten_ni r0=18.16 cs=0.403e6 s=1.237
           g0=1.67 cv=1.66e10
endeos
*
*eor* cthin
*
nose shape tests: ogive v=1474 target=7039 al finite
*
control
    tstop 300.e-6
    rdumpf 3600

```

```

    cpshift 999.
endcontrol
*
restart
* file='rsct1'
  time=0.e-6
endr
*
cellthermo
  mmp
  ntbad=99999
endc
*
convct
*
* NOTE: if KE Sim convection=0, if MV Sim convection=1
*
  convection=0
  interface=high_resolution
endconvct
*
edit
  shortt
    time 0. dtfrequency 150.e-6
  ends
  longt
    time 0. dtfrequency 600.e-6
  endl
  plott
    time 0. dtfrequency 50.e-6
  endp
  histt
    time 0. dtfrequency 0.3e-6
  htracer1
  htracer2
  htracer3
  htracer4
  htracer5
  htracer6
  htracer7
  htracer8
  htracer9
  htracer10
endh
ende

```

```

*
boundary
  bhydro
    block 1
      bxbot 0
      bxtop 2
      bybot 2
      bytop 2
    endb
  endh
endb
*
fracts
  pressure
  pfrac1 -5.0e9
  pfrac2 -35.0e9
  pfmix -1.0e20
  pfvoid -1.0e20
endf
*
*eor* pltinp
*

```

INTENTIONALLY LEFT BLANK.

Appendix E:

Input for Hemi-Nose KE-BL-CO-S Sims vs. 5083 Aluminum Targets

INTENTIONALLY LEFT BLANK.

```

* Run History
*
*eor* cgenin
*
nose shape tests: hemi v=1147 target=5083 al finite
*
control
  ep
  mmp
  viscosity bl=.1 bq=2 bs=0.1
endcontrol
*
mesh
  block 1 geom=2dc type=e
    x0 0.00
    x1 n 40 w 1.6891 rat 1.0
    x2 n 45 dxf 0.0422275 rat 1.05
  endx
  y0 -10.219055
  y1 n 832 dyf 0.0422275 rat 1.0
  endy
  xactive 0.0 0.4
  yactive -10.219055 0.0
endblock
endmesh
*
insertion
  block 1
    package '5083 Al target'
    material 1
    numsub 50
    insert box
      p1=0.0 0.0
      p2=7.6 7.62
    endinsert
  endpackage
  package 'w alloy rod nose'
  material 2
  numsub 100
*
* NOTE: striking velocity (yvel) is changed below
*
  yvel 1.147e5
  insert circle
    ce=0.0 -0.33782

```

```

    r= 0.33782
endinsert
endpackage
package 'w alloy rod body'
material 2
numsub 50
*
* NOTE: striking velocity (yvel) is changed below
*
    yvel 1.147e5
    insert box
        p1=0.0  -0.33782
        p2=0.33782 -10.1346
    endinsert
endpackage
endblock
endinsertion
*
epdata
vpsave
*
* NOTE: poisson ratio from for Tungsten from Metals Handbook, that for 5083
*       Aluminum from Forrestal, M.J., V. K. Luk, and N. S. Brar, "Perforation of
*       aluminum with conical-nose projectiles", Mechanic and Materials 10 (1990)
*       pp. 97-105.
*
* NOTE: properties for 5083 aluminum from Silling, S. A., "CTH Reference Manual:
*       Boundary Layer Algorithm for Sliding Interfaces in Two Dimensions", Sandia
*       National Laboratories Report SAND93-2487, January 1994.
*
* NOTE: 5083 aluminum using undocumented power law
*
    matep 1
    johnson-cook='USER'
        ajo=-2.76e9 bjo=254.7  cjo=0.0
        mjo=1.0   njo=0.084  tjo=6.68e-2
        poisson 0.333
*
* NOTE: for strain failure at 150% all parameter for Johnson-Cook fracture model except
*       the first are set to zero.
*
        jfrac='USER' jfd1=1.5 jfd2=0.0 jfd3=0.0 jfd4=0.0 jfd5=0.0
        jftm=0.0 jfpf0=-4.5e9
*
* NOTE: actual tungsten alloy was 95W-2.5Ni-1.0Fe-1.5Co (21% swaged) with r0=18.1.

```

```

*      95W-3.5Ni-1.5Fe is being used to approximate the w alloy.
*
matep 2
  steinberg='TUNGSTEN_NI_FE'
    r0st=18.16  tm0st=0.195002  atmst=1.3
    gm0st=1.67  ast=1.03e-12  bst=1.76396
    nst=0.13   c1st=0.0       c2st=0.0
    g0st=1.45e12  btst=7.7     eist=0.0
    ypst=0.0     ukst=0.0     ysmst=0.0
    yast=0.0     y0st=18.7e9   ymst=40.e9
    poisson=0.280
*
* NOTE: for strain failure at 150% all parameter for Johnson-Cook fracture model except
*       the first are set to zero.
*
      jfrac='USER' jfd1=1.5 jfd2=0.0 jfd3=0.0 jfd4=0.0 jfd5=0.0
      jftm=0.0 jfpf0=-35.e9
*
* NOTE: parameters for boundary layer algorithm taken similar to:
*       Kmetyk, L. N. and P. Yarrington, "CTH Analysis of Steel Rod Penetration
*       Into Aluminum and Concrete Targets with Comparisons to Experimental Data",
*       Sandia National Laboratories Report SAND94-1498, October 1994.
*
* NOTE: if no BLINT model, next line is commented out. If no yield strength correction
*       factor 'corr' is omitted
*
      blint 1 soft 1 hard 2 wsl 0.084455 wbl 0.084455 fric=0.0 corr
      mix 3
endep
*
tracer
  block 1
    add 0. 0. to 0. -10.134 n 10
endtracer
*
edit
  block 1
    noexpanded
  endblock
endedit
*
eos
*
* NOTE: EOS properties from cth mgrun library
*

```

```

* NOTE: 5083-H131 Aluminum eos approximated with 6061-t6 Aluminum
*       density reduced to reflect that for 5083 Aluminum from
*       Metal's Handbook.
*
mat1 mgrun eos=6061-t6_al r0=2.66 cs=0.534e6 s=1.4
      g0=1.97 cv=1.07e11
mat2 mgrun eos=tungsten_ni r0=18.16 cs=0.403e6 s=1.237
      g0=1.67 cv=1.66e10
endeos
*
*eor* cthin
*
nose shape tests: hemi v=1147 target=5083 al finite
*
control
  tstop 300.e-6
  rdumpf 3600
  cpshift 999.
endcontrol
*
restart
* file='rsct1'
  time=0.e-6
endr
*
cellthermo
  mmp
  ntbad=99999
endc
*
convct
*
* NOTE: if KE Sim convection=0, if MV Sim convection=1
*
  convection=0
  interface=high_resolution
endconvct
*
edit
  shortt
    time 0. dtfrequency 150.e-6
  ends
  longt
    time 0. dtfrequency 600.e-6
  endl

```

```

plott
  time 0. dtfrequency 50.e-6
endp
histt
  time 0. dtfrequency 0.3e-6
  htracer1
  htracer2
  htracer3
  htracer4
  htracer5
  htracer6
  htracer7
  htracer8
  htracer9
  htracer10
endh
ende
*
boundary
  bhydro
    block 1
    bxbot 0
    bxtop 2
    bybot 2
    bytop 2
  endb
endh
endb
*
fracts
  pressure
  pfrac1 -4.5e9
  pfrac2 -35.0e9
  pfmix -1.0e20
  pfvoid -1.0e20
endf
*
*eor* pltinp
*
```

INTENTIONALLY LEFT BLANK.

Appendix F:

Input for Ogival-Nose KE-BL-CO-S Sims vs. 5083 Aluminum Targets

INTENTIONALLY LEFT BLANK.

```

* Run History
*
*eor* cgenin
*
nose shape tests: ogive v=1286 target=5083 al finite
*
control
  ep
  mmp
  viscosity bl=.1 bq=2 bs=0.1
endcontrol
*
mesh
  block 1 geom=2dc type=e
    x0 0.00
    x1 n 40 w 1.6891 rat 1.0
    x2 n 45 dxf 0.0422275 rat 1.05
  endx
  y0 -10.219055
  y1 n 832 dyf 0.0422275 rat 1.0
  endy
  xactive 0.0 0.4
  yactive -10.219055 0.0
endblock
endmesh
*
insertion
  block 1
    package '5083 Al target'
    material 1
    numsub 50
    insert box
    p1=0.0 0.0
    p2=7.6 7.62
    endinsert
  endpackage
  package 'w alloy ogive nose rod'
  material 2
  numsub 100
*
* NOTE: striking velocity (yvel) is changed below
*
  yvel 1.286e5
  insert uds
  point 0.0 0.0

```

```

point 0.050437038 -0.08003015622
point 0.095867718 -0.1600603124
point 0.136665799 -0.2400904687
point 0.173135779 -0.3201206249
point 0.205527612 -0.4001507811
point 0.234047376 -0.4801809373
point 0.258865148 -0.5602110935
point 0.280120900 -0.6402412498
point 0.297928948 -0.7202714060
point 0.312381319 -0.8003015622
point 0.323550306 -0.8803317184
point 0.331490355 -0.9603618746
point 0.336239443 -1.040392031
point 0.337820 -1.120422187
point 0.337820 -10.1346
point 0.0 -10.1346
point 0.0 0.0
endinsert
endpackage
endblock
endinsertion
*
epdata
vpsave
*
* NOTE: poisson ratio from for Tungsten from Metals Handbook, that for 5083
* Aluminum from Forrestal, M.J., V. K. Luk, and N. S. Brar, "Perforation of
* aluminum with conical-nose projectiles", Mechanic and Materials 10 (1990)
* pp. 97-105.
*
* NOTE: properties for 5083 aluminum from Silling, S. A., "CTH Reference Manual:
* Boundary Layer Algorithm for Sliding Interfaces in Two Dimensions", Sandia
* National Laboratories Report SAND93-2487, January 1994.
*
* NOTE: 5083 aluminum using undocumented power law
*
matep 1
johnson-cook='USER'
      ajo=-2.76e9 bjo=254.7 cjo=0.0
      mjo=1.0 njo=0.084 tjo=6.68e-2
      poisson 0.333
*
* NOTE: for strain failure at 150% all parameter for Johnson-Cook fracture model except
* the first are set to zero.
*

```

```

jfrac='USER' jfd1=1.5 jfd2=0.0 jfd3=0.0 jfd4=0.0 jfd5=0.0
jftm=0.0 jfpf0=-4.5e9
*
* NOTE: actual tungsten alloy was 95W-2.5Ni-1.0Fe-1.5Co (21% swaged) with r0=18.1.
* 95W-3.5Ni-1.5Fe is being used to approximate the w alloy.
*
matep 2
steinberg='TUNGSTEN_NI_FE'
r0st=18.16 tm0st=0.195002 atmst=1.3
gm0st=1.67 ast=1.03e-12 bst=1.76396
nst=0.13 c1st=0.0 c2st=0.0
g0st=1.45e12 btst=7.7 eist=0.0
ypst=0.0 ukst=0.0 ysmst=0.0
yast=0.0 y0st=18.7e9 ymst=40.e9
poisson=0.280
*
* NOTE: for strain failure at 150% all parameter for Johnson-Cook fracture model except
* the first are set to zero.
*
jfrac='USER' jfd1=1.5 jfd2=0.0 jfd3=0.0 jfd4=0.0 jfd5=0.0
jftm=0.0 jfpf0=-35.e9
*
* NOTE: parameters for boundary layer algorithm taken similar to:
* Kmetyk, L. N. and P. Yarrington, "CTH Analysis of Steel Rod Penetration
* Into Aluminum and Concrete Targets with Comparisons to Experimental Data",
* Sandia National Laboratories Report SAND94-1498, October 1994.
*
* NOTE: if no BLINT model, next line is commented out. If no yield strength correction
* factor 'corr' is omitted
*
blint 1 soft 1 hard 2 wsl 0.084455 wbl 0.084455 fric=0.0 corr
mix 3
endep
*
tracer
block 1
add 0. 0. to 0. -10.1345 n 10
endtracer
*
edit
block 1
noexpanded
endblock
endedit
*

```

```

eos
*
* NOTE: EOS properties from cth mgrun library
*
* NOTE: 5083-H131 Aluminum eos approximated with 6061-t6 Aluminum
*       density reduced to reflect that for 5083 Aluminum from
*       Metal's Handbook.
*
mat1 mgrun eos=6061-t6_al r0=2.66  cs=0.534e6  s=1.4
          g0=1.97  cv=1.07e11
mat2 mgrun eos=tungsten_ni r0=18.16  cs=0.403e6  s=1.237
          g0=1.67  cv=1.66e10
endeos
*
*eor* cthin
*
nose shape tests: ogive v=1286 target=5083 al finite
*
control
  tstop 300.e-6
  rdumpf 3600
  cpshift 999.
endcontrol
*
restart
* file='rsct1'
  time=0.e-6
endr
*
cellthermo
  mmp
  ntbad=99999
endc
*
convct
*
* NOTE: if KE Sim convection=0, if MV Sim convection=1
*
  convection=0
  interface=high_resolution
endconvct
*
edit
shortt
  time 0. dtfrequency 150.e-6

```

```

ends
longt
  time 0. dtfrequency 600.e-6
endl
plott
  time 0. dtfrequency 50.e-6
endp
histt
  time 0. dtfrequency 0.3e-6
  htracer1
  htracer2
  htracer3
  htracer4
  htracer5
  htracer6
  htracer7
  htracer8
  htracer9
  htracer10
endh
ende
*
boundary
  bhydro
    block 1
      bxbot 0
      bxtop 2
      bybot 2
      bytop 2
    endb
  endh
endb
*
fracts
  pressure
  pfrac1 -4.5e9
  pfrac2 -35.0e9
  pfmix -1.0e20
  pfvoid -1.0e20
endf
*
*eor* pltinp
*
```

INTENTIONALLY LEFT BLANK.

Appendix G:
Table of Simulation Results

INTENTIONALLY LEFT BLANK.

KE-BL-CO-P Sims vs. 5083 Aluminum Targets					
65 g Hemi-Nose Rods (id=3)			63 g Ogival-Nose Rods (id=2)		
Striking Velocity (m/s)	Residual Velocity (m/s)	Comments	Striking Velocity (m/s)	Residual Velocity (m/s)	Comments
1147	1026	rigid	1286	1145	rigid
1201	1027	eroded	1399	1296	rigid
1283	1090	eroded	1534	1432	rigid
			1600	1510	rigid
			1800	1730	rigid
			1900	1828	rigid
			2000	1909	deformed
			2100	1938	eroded
KE-BL-CO-P Sim vs. 7039 Aluminum Targets					
65 g Hemi-Nose Rods (id=3)			63 g Ogival-Nose Rods (id=2)		
Striking Velocity (m/s)	Residual Velocity (m/s)	Comments	Striking Velocity (m/s)	Residual Velocity (m/s)	Comments
1038	737	rigid	1474	1344	rigid
1093	910	deformed	1595	1454	rigid
1198	915	eroded	1800	1697	rigid
			1900	1774	deformed
			2000	1820	eroded
MV-BL-CO-P Sims vs. 5083 Aluminum Targets					
65 g Hemi-Nose Rods (id=4)			63 g Ogival-Nose Rods (id=3)		
Striking Velocity (m/s)	Residual Velocity (m/s)	Comments	Striking Velocity (m/s)	Residual Velocity (m/s)	Comments
1147	973	rigid	1286	1082	rigid
1201	1084	rigid	1399	1243	rigid
1283	1151	deformed	1534	1405	rigid
			1600	1460	rigid
MV-BL-CO-P Sims vs. 7039 Aluminum Targets					
65 g Hemi-Nose Rods (id=4)			63 g Ogival-Nose Rods (id=3)		
Striking Velocity (m/s)	Residual Velocity (m/s)	Comments	Striking Velocity (m/s)	Residual Velocity (m/s)	Comments
1038	744	rigid	1474	1310	rigid
1093	796	rigid	1595	1399	rigid
1198	1007	deformed			

KE-NB-NC-P Sims vs. 5083 Aluminum Targets					
65 g Hemi-Nose Rods (id-5)			63 g Ogival-Nose Rods (id-4)		
Striking Velocity (m/s)	Residual Velocity (m/s)	Comments	Striking Velocity (m/s)	Residual Velocity (m/s)	Comments
1147	726	eroded, excessively deformed	1600	1375	eroded
1283	930	eroded, excessively deformed			
KE-BL-CO-S Sims vs. 5083 Aluminum Targets					
65 g Hemi-Nose Rods (id-6)			63 g Ogival-Nose Rods (id-5)		
Striking Velocity (m/s)	Residual Velocity (m/s)	Comments	Striking Velocity (m/s)	Residual Velocity (m/s)	Comments
1147	927	rigid	1286	1043	rigid
1201	1041	eroded	1399	1186	rigid
1283	1021	eroded	1534	1339	rigid
			1600	1439	rigid
KE-BL-NC-P Sims vs. 5083 Aluminum Targets					
65 g Hemi-Nose Rods (id-7)			63 g Ogival-Nose Rods (id-6)		
Striking Velocity (m/s)	Residual Velocity (m/s)	Comments	Striking Velocity (m/s)	Residual Velocity (m/s)	Comments
1147	828	eroded, excessively deformed	1286	1123	nose deformed slightly
1201	870	eroded, excessively deformed	1399	1292	nose deformed
1283	1007	eroded, excessively deformed	1534	1326	eroded
			1600	1420	eroded

**NO. OF
COPIES ORGANIZATION**

2 DEFENSE TECHNICAL
INFORMATION CENTER
DTIC DDA
8725 JOHN J KINGMAN RD
STE 0944
FT BELVOIR VA 22060-6218

1 HQDA
DAMO FDQ
DENNIS SCHMIDT
400 ARMY PENTAGON
WASHINGTON DC 20310-0460

1 DPTY ASSIST SCY FOR R&T
SARD TT F MILTON
RM 3EA79 THE PENTAGON
WASHINGTON DC 20310-0103

1 OSD
OUSD(A&T)/ODDDR&E(R)
J LUPO
THE PENTAGON
WASHINGTON DC 20301-7100

1 CECOM
SP & TRRSTRL COMMCTN DIV
AMSEL RD ST MC M
H SOICHER
FT MONMOUTH NJ 07703-5203

1 PRIN DPTY FOR TCHNLGY HQ
US ARMY MATCOM
AMCDCG T
M FISETTE
5001 EISENHOWER AVE
ALEXANDRIA VA 22333-0001

1 PRIN DPTY FOR ACQUSTN HQS
US ARMY MATCOM
AMCDCG A
D ADAMS
5001 EISENHOWER AVE
ALEXANDRIA VA 22333-0001

1 DPTY CG FOR RDE HQS
US ARMY MATCOM
AMCRD
BG BEAUCHAMP
5001 EISENHOWER AVE
ALEXANDRIA VA 22333-0001

**NO. OF
COPIES ORGANIZATION**

1 INST FOR ADVNCD TCHNLGY
THE UNIV OF TEXAS AT AUSTIN
PO BOX 202797
AUSTIN TX 78720-2797

1 USAASA
MOAS AI W PARRON
9325 GUNSTON RD STE N319
FT BELVOIR VA 22060-5582

1 CECOM
PM GPS COL S YOUNG
FT MONMOUTH NJ 07703

1 GPS JOINT PROG OFC DIR
COL J CLAY
2435 VELA WAY STE 1613
LOS ANGELES AFB CA 90245-5500

1 ELECTRONIC SYS DIV DIR
CECOM RDEC
J NIEMELA
FT MONMOUTH NJ 07703

3 DARPA
L STOTTS
J PENNELLA
B KASPAR
3701 N FAIRFAX DR
ARLINGTON VA 22203-1714

1 USAF SMC/CED
DMA/JPO
M ISON
2435 VELA WAY STE 1613
LOS ANGELES AFB CA
90245-5500

1 US MILITARY ACADEMY
MATH SCI CTR OF EXCELLENCE
DEPT OF MATHEMATICAL SCI
MDN A MAJ DON ENGEN
THAYER HALL
WEST POINT NY 10996-1786

1 DIRECTOR
US ARMY RESEARCH LAB
AMSRL CS AL TP
2800 POWDER MILL RD
ADELPHI MD 20783-1145

NO. OF
COPIES ORGANIZATION

- 1 DIRECTOR
US ARMY RESEARCH LAB
AMSRL CS AL TA
2800 POWDER MILL RD
ADELPHI MD 20783-1145
- 3 DIRECTOR
US ARMY RESEARCH LAB
AMSRL CI LL
2800 POWDER MILL RD
ADELPHI MD 20783-1145

ABERDEEN PROVING GROUND

- 4 DIR USARL
AMSRL CI LP (305)

NO. OF COPIES	ORGANIZATION
6	CDR US ARMY ARDEC AMSTA AR AEE WW E BAKER C CHIN R FONG J PEARSON J WALSH TECH LIB PICATINNY ARSENAL NJ 07806-5000
1	CDR US ARMY ARDEC AMSTA AR AET M TECH LIB PICATINNY ARSENAL NJ 07806-5000
1	CDR US ARMY ARDEC AMSTA AR FS E ANDRICOPOULOS PICATINNY ARSENAL NJ 07806-5000
3	CDR US ARMY MERDEC AMSME RD ST WF L CRAFT D LOVELACE M SCHEXNAYDER REDSTONE ARSENAL AL 35898-5250
1	DIR US ARO WASH AMXRO W K A BANNISTER RM 8N31 5001 EISENHOWER AVE ALEXANDRIA VA 22333-0001
3	DIR US ARO J CHANDRA K IYER TECH LIB PO BOX 12211 RESEARCH TRIANGLE PARK NC 27709-2211
3	DIR US ARMY DARPA J RICHARDSON TECH INFO B WILCOX 3701 N FAIRFAX DR ARLINGTON VA 22203-1714

NO. OF COPIES	ORGANIZATION
4	CDR US ARMY COE J BALSARA T BLEVINS P PAPIDOS R NAMBURA 3909 HALL FERRY RD VICKSBURG MS 39180-6199
2	CDR US ARMY TACOM AMSTA RSK J THOMPSON S GOODMAN WARREN MI 48397-5000
2	DIR NRL J A NEMES A E WILLIAMS CODE 6684 4555 OVERLOOK AVE SW WASHINGTON DC 20375
2	CDR NSWC W H HOLT CODE G22 W MOCK 17320 DAHLGREN RD DAHLGREN VA 22448-5000
8	CDR NSWC C S COFFEY R K GARRETT JR H MAIR R12 J MCKIRGAN B PARK D G TASKER TECH LIB F ZERILLI 10901 NEW HAMPSHIRE AVE SILVER SPRING MD 20903-5000
2	CDR NWC T GILL CODE 3261 TECH LIB CHINA LAKE CA 93555-6001
1	NAVAL POST GRAD SCHL J STERNBERG CODE 73 MONTEREY CA 93943
1	USAF PHILLIPS LAB PL WSCD F ALLAHADADI KIRKLAND AFB NM 87185

NO. OF
COPIES ORGANIZATION

1 USAF WAL
T NICHOLAS
WRIGHT PAT AFB OH 45433

4 USAF WL
MNMW W COOK
J FOSTER
M NIXON
TECH LIB
EGLIN AFB FL 32542-5434

14 DIR LANL
T F ADAMS F663
J BOLSTAD G787
J CHAKYAK
R DAVIDSON K557
E FERM
P FOLLANSBEE F663
G T GRAY III B295
K HOLIAN B295
L HULL
J JOHNSON F663
D A MANDELL F663
P MAULIN
L SCHWALBE
TECH LIB
PO BOX 1663
LOS ALAMOS NM 87454

11 DIR LLNL
R COUCH L35
M FINGER L38
W H GOURDIN
G GOUDREAU
C HOOVER
D LASSILA L342
P RABOIN
J E REAUGH L290
M J MURPHY
TECH LIB
R E TIPTON L35
PO BOX 808
LIVERMORE CA 94550

1 DIR LLNL
C KLINE L017
PHYSICS DEPT
PO BOX 808
LIVERMORE CA 94550

NO. OF
COPIES ORGANIZATION

2 DIR SNL
D BAMMANN
M CHIESA
LIVERMORE CA 94550

9 DIR SNL
R M BRANNON DIV 1432
L C CHHABILDAS MS 0821
M FORRESTAL DIV 1551
E S HERTEL JR MS 0819
M KIPP DIV 1533
J M MCGLAUN MS 0819
S A SILLING
T TRUCANO MS 0819
P YARRINGTON DIV 1533
PO BOX 5800
ALBUQUERQUE NM 87185-0307

5 IAT
UNIV OF TX AUSTIN
S J BLESS
H D FAIR
T M KIEHNE
M J NORMANDIA
D LITTLEFIELD
4030 2 W BRAKER LN
AUSTIN TX 78759-5329

3 SOUTHWEST RSCH INST
C ANDERSON
S MULLIN
J WALKER
8500 CULEBRA RD
PO DRAWER 28510
SAN ANTONIO TX 78284

1 AEROJET ELECTRO SYS CO
WARHEAD SYSTEMS
J CARLEONE
PO BOX 296
AZUSA CA 91702

1 APPLIED RSCH ASSOC INC
J D YATTEAU
5941 S MIDDLEFIELD RD STE 100
LITTLETON CO 80123

**NO. OF
COPIES ORGANIZATION**

2 APPLIED RSCH ASSOC INC
T C CARNEY
F MAESTAS
4300 SAN MATEO BLVD SE
STE A220
ALBUQUERQUE NM 87110

1 BRIGS CO
J E BACKOFEN
2668 PETERSBOUGH ST
HERNDON VA 22071-2443

3 DYNA EAST CORP
P C CHOU
R CICCARELLI
W FLIS
3620 HORIZON DRIVE
KING OF PRUSSIA PA 19406

2 GEN RSCH CORP
ATTN A CHARTERS
T MENNA
5383 HOLLISTER AVE
SANTA BARBARA CA 93111

1 IRA INC
D ORPHAL
4450 BLACK AVE STE E
PLEASANTON CA 94566

1 KAMAN SCIENCES CORP
J S WILBECK
7600 BLVD S STE 208
HUNTSVILLE AL 35802

1 KAMAN SCIENCES CORP
N ARI
PO BOX 7463
COLORADO STRINGS CO 80933-7463

1 D R KENNEDY & ASSOC INC
D KENNEDY
PO BOX 4003
MOUNTAIN VIEW CA 94040

1 KERLEY PUB SVC
G I KERLEY
PO BOX 13835
ALBUQUERQUE NM 87192-3835

**NO. OF
COPIES ORGANIZATION**

3 LIVERMORE SOFTWARE
TECH CORP
J O HALLQUIST
B MAKER
D STILLMAN
2876 WAVERLY WAY
LIVERMORE CA 94550

1 ORLANDO TECH INC
D A MATUSKA
PO BOX 855
SHALIMAR FL 32579

2 SRI INTERNATIONAL
D CURRAN
L SEAMAN
333 RAVENSWOOD AVE
MENLO PARK CA 94025

1 ZERNOW TECH SVC INC
L ZERNOW
425 W BONITA AVE STE 208
SAN DIMAS CA 91773

1 COMPUTATIONAL MECH ASSOC
J A ZUKAS
PO BOX 11314
BALTIMORE MD 21239-0314

4 ALLIANT TECHSYS INC
S BEISSEL
T HOLMQUIST MN11 2720
R STRYK
G R JOHNSON MN11 2925
600 SECOND ST NE
HOPKINS MN 55343

ABERDEEN PROVING GROUND

1 DIR AMSAA
R THOMPSON

53 DIR USARL
AMSRL SL B, P DIETZ (328)
AMSRL SL BC, J T KOLPCIC (328)
AMSRL SL BV,
R SAUCIER (247)
R SHNIDMAN (247)
J R STROBEL (247)

NO. OF
COPIES ORGANIZATION

AMSRL WM, D ECCLESHALL
 AMSRL WM MA S, J BEATTY
 S CHOU
 J DANDEKAR
 D J GROVE
 A RAJENDRAN
 T WEERASOORIYA
 AMSRL WM PD,
 G GAZONAS
 D HOPKINS
 S WILKERSON
 AMSRL WM T, W MORRISON
 AMSRL WM TA,
 W BRUCHEY JR
 G FILBEY JR
 W GILLICH
 W GOOCH JR
 Y HAUNG
 H MEYER JR
 J DEHN
 S BILYK
 E RAPACKI JR
 AMSRL WM TB,
 R FREY
 J STARKENBERG
 R LOTTERO
 AMSRL WM TC,
 R COATES
 W S DE ROSSET
 F GRACE
 K KIMSEY
 M LAMPSON
 S SCHRAML
 L MAGNESS
 W WALTERS
 D SCHEFFLER (4 CP)
 AMSRL WM TD,
 R L BITTING
 A M DIETRICH JR
 T FARRAND
 K FRANK
 N GNIAZDOWSKI
 F GREGORY
 P KINGMAN
 M RAFTENBERG
 M SCHEIDLER
 S SCHOENFELD
 S SEGLETES
 J WALTER JR
 T W WRIGHT

REPORT DOCUMENTATION PAGE			Form Approved OMB No. 0704-0188	
<small>Public reporting burden for this collection of information is estimated to average 1 hour per response, including the time for reviewing instructions, searching existing data sources, gathering and maintaining the data needed, and completing and reviewing the collection of information. Send comments regarding this burden estimate or any other aspect of this collection of information, including suggestions for reducing this burden, to Washington Headquarters Services, Directorate for Information Operations and Reports, 1215 Jefferson Davis Highway, Suite 1204, Arlington, VA 22202-4302, and to the Office of Management and Budget, Paperwork Reduction Project(0704-0188), Washington, DC 20503.</small>				
1. AGENCY USE ONLY (Leave blank)		2. REPORT DATE January 1998		3. REPORT TYPE AND DATES COVERED Final, July 1995 - May 1997
4. TITLE AND SUBTITLE Modeling Threshold Velocity of Hemispherical and Ogival-Nose Tungsten-Alloy Penetrators Perforating Finite Aluminum-Targets			5. FUNDING NUMBERS PR: 1L162618AH80	
6. AUTHOR(S) Daniel R. Scheffler				
7. PERFORMING ORGANIZATION NAME(S) AND ADDRESS(ES) U.S. Army Research Laboratory ATTN: AMSRL-WM-TC Aberdeen Proving Ground, MD 21005-5066			8. PERFORMING ORGANIZATION REPORT NUMBER ARL-TR-1583	
9. SPONSORING/MONITORING AGENCY NAMES(S) AND ADDRESS(ES)			10.SPONSORING/MONITORING AGENCY REPORT NUMBER	
11. SUPPLEMENTARY NOTES				
12a. DISTRIBUTION/AVAILABILITY STATEMENT Approved for public release; distribution is unlimited.			12b. DISTRIBUTION CODE	
13. ABSTRACT (Maximum 200 words) This study examines the ability of the CTH hydrocode to predict the effect of rod nose-shape on the transition from rigid body to eroding rod penetration for tungsten alloy long-rod penetrators perforating finite aluminum targets. Two rod nose-shapes and two target alloys were considered. The rod nose-shapes were hemispherical and ogival, and the target alloys were 7.62-cm-thick 5083 and 7039 aluminum. Results are compared to an experimental study that delineated the effect of nose-shape on the threshold velocity at which tungsten alloy penetrators transition from rigid body to eroding rod when perforating finite aluminum targets.				
14. SUBJECT TERMS penetrator, impact, hydrocode, perforation, rigid body penetrator, tungsten, aluminum, threshold velocity			15. NUMBER OF PAGES 85	
			16. PRICE CODE	
17. SECURITY CLASSIFICATION OF REPORT UNCLASSIFIED	18. SECURITY CLASSIFICATION OF THIS PAGE UNCLASSIFIED	19. SECURITY CLASSIFICATION OF ABSTRACT UNCLASSIFIED	20. LIMITATION OF ABSTRACT UL	

INTENTIONALLY LEFT BLANK.

USER EVALUATION SHEET/CHANGE OF ADDRESS

This Laboratory undertakes a continuing effort to improve the quality of the reports it publishes. Your comments/answers to the items/questions below will aid us in our efforts.

1. ARL Report Number/Author ARL-TR-1583 (Scheffler) Date of Report January 1998

2. Date Report Received _____

3. Does this report satisfy a need? (Comment on purpose, related project, or other area of interest for which the report will be used.) _____

4. Specifically, how is the report being used? (Information source, design data, procedure, source of ideas, etc.) _____

5. Has the information in this report led to any quantitative savings as far as man-hours or dollars saved, operating costs avoided, or efficiencies achieved, etc? If so, please elaborate. _____

6. General Comments. What do you think should be changed to improve future reports? (Indicate changes to organization, technical content, format, etc.) _____

CURRENT
ADDRESS

Organization

Name

E-mail Name

Street or P.O. Box No.

City, State, Zip Code

7. If indicating a Change of Address or Address Correction, please provide the Current or Correct address above and the Old or Incorrect address below.

OLD
ADDRESS

Organization

Name

Street or P.O. Box No.

City, State, Zip Code

(Remove this sheet, fold as indicated, tape closed, and mail.)
(DO NOT STAPLE)

DEPARTMENT OF THE ARMY

OFFICIAL BUSINESS

BUSINESS REPLY MAIL
FIRST CLASS PERMIT NO 0001,APG,MD

POSTAGE WILL BE PAID BY ADDRESSEE

DIRECTOR
US ARMY RESEARCH LABORATORY
ATTN AMSRL WM TC
ABERDEEN PROVING GROUND MD 21005-5066



NO POSTAGE
NECESSARY
IF MAILED
IN THE
UNITED STATES

